Study of CHEC-S TARGET C Module Trigger Performance

Bachelorarbeit aus der Physik

Vorgelegt von
Markus Reif
14. August 2017

Erlangen Centre for Astroparticle Physics
Physikalisches Institut II
Friedrich-Alexander-Universität Erlangen-Nürnberg

Betreuer: Prof. Dr. Stefan Funk

Abstract

The Cherenkov Telescope Array (CTA) is a future Imaging Air Cherenkov Telescope (IACT), designed to detect gamma-rays from 30 GeV to 300 TeV. It will consist out of three different types of telescopes. Large-, medium- and small-sized telescopes, covering different energy ranges. A proposed layout for the small-sized telescopes is a GCT[1]. GCTs will use a CHEC[2] system based on the Target[3] C module with the two ASICs [4] T5TEA[5] providing triggering and Target C providing digitization. In this thesis the results of systematic parameters scans with the Target C module, to study the trigger performance, will be presented. All 64 channel of the module are able to trigger on thresholds < 3 mV with 50% efficiency and a mean of (2.436 ± 0.020) mV.
Additionally the spread between the channels of a triggergroup was examined, being smaller than 5% for all channels, except for channel 5 at low thresholds ($\sim$10 mV), where the deviation is (6.02 ± 0.13) %.

[1] Gamma-ray Cherenkov Telescope
[2] Compact High Energy Camera
[3] TeV Array Readout Electronics with GaS/s sampling and Event Trigger [17]
[4] Application Specific integrated Circuit
[5] Target 5 Trigger Extension ASIC [19, page 13]

Contents

1 Introduction

Gamma-rays make up the high energy end of electromagnetic radiation, with energies even higher than x-rays (see Figure 1).

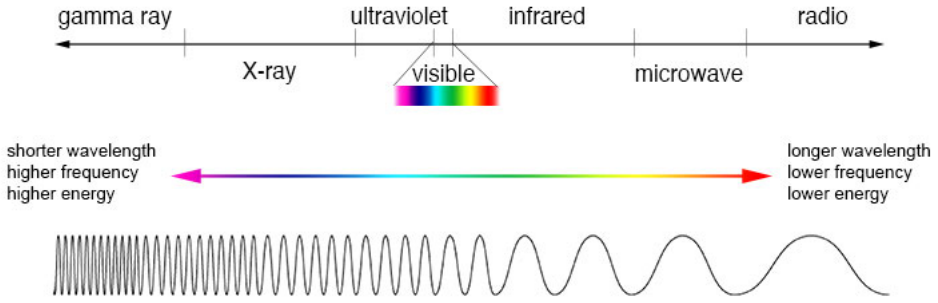

Figure 1: Electromagnetic spectrum [1]

Gamma-ray astronomy tries to detect these photons. It is a rather new branch of astronomy, having its beginnings in 1961, when the first gamma-ray telescope was carried into the orbit on the Explorer 11 satellite [2]. By measuring gamma-rays we want to learn something about which processes in our universe can produce such high energy photons. Possible sources of gamma radiation are supernovae, neutron stars or active galactic nuclei (AGN). In our laboratories on earth we are not able to produce photons with such high energies, therefore gamma-rays, from the universe, offer us the possibility to test theories and investigate physics in the high energy regime [2].
Apart from increasing our knowledge in physics, gamma-ray astronomy also pushes forward our technical abilities, because if we want to get better results than previous experiments we need to upgrade our detectors. This led to the Target ASICs T5TEA and Target C, being part of the Target C module (see Section 4). This module will be used in cameras of telescopes of the Cherenkov Telescope Array to do the triggering (T5TEA) and digitization (Target C). The trigger performance of the Target C module was investigated in this thesis.

2 Detection Of Cosmic Gamma-Rays

To draw conclusion about where gamma-rays come from and what their sources are, we need to detect them. For this we currently have two opportunities.

2.1 Space-Based Telescopes

Gamma-rays are absorbed in earth's atmosphere, hence we can bring our telescopes into space. Presents most advanced gamma-ray space telescope is the 'Large Area Telescope' (LAT) on the Fermi satellite (originally 'GAMMA-RAY LARGE AREA SPACE TELESCOPE', GLAST)(see Fig. 2), which was launched in 2008. [3, page 16]

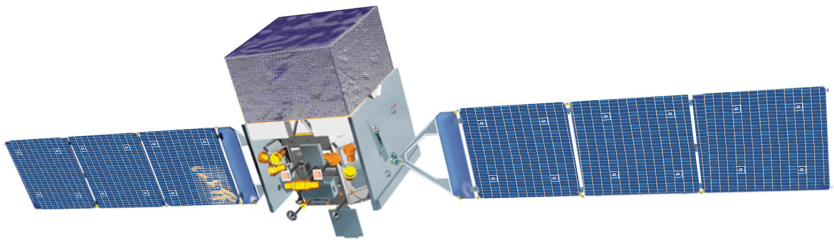

Figure 2: Illustration of the Fermi-/GLAST-satellite [4]

The LAT is able to detect electromagnetic radiation with energies from 30 MeV to more than 300 GeV [3, page 33].
Until today Fermi has discovered more than 200 pulsars, found out that thermonuclear explosions on the surface of stars can produce gamma-rays and even explored gamma-ray sources close to the earth, like thunderstorms in the earth's atmosphere, solar flares and even charged particles hitting the surface of the moon. [5]

2.2 Ground-Based Telescopes

Space based telescopes get inefficient in detecting gamma-rays in the very high energy (VHE) range, because the flux of the gamma-rays decreases with increasing energies. Hence, a large detection area is needed, to measure a significant amount of photons. To detect VHE gamma-rays, we can use the atmosphere, which has a large volume compared to satellites, as part of the detector. This is done in ground based telescopes. As mentioned before, gamma-rays are absorbed in the atmosphere, which means that the photon loses its energy by interacting with particles of the atmosphere. There are three absorption processes, the photoelectric effect, Compton scattering and pair production, depending on the energy of the incoming photon.

2.2.1 Extensive Air Showers

For gamma energies higher than 10 MeV pair production is the dominating effect, and an electromagnetic shower is created. This happens in the following steps (compare Fig. 3). A high energetic gamma-ray interacts with a nucleus of the atmosphere. In this process an electron-positron-pair is created via pair-production. The occurring particles then create new gamma-rays by losing their energy via Bremsstrahlung by interacting with other nuclei of the atmosphere. These secondary photons can create, if they have enough energy, new electron-positron-pairs. This exponential process continues until the ionization losses of the electrons and positrons are equal to the losses due to Bremsstrahlung [7, page 6].

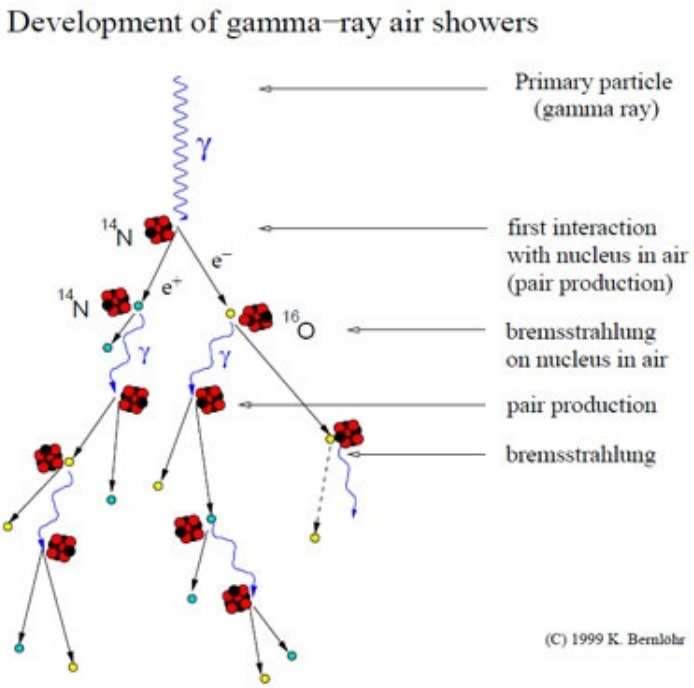

Figure 3: Schematic of a gamma-ray induced air shower [6]

2.2.2 Cherenkov Effect

If the electrons or positrons of the air shower exceed a certain velocity, the Cherenkov effect occurs. This effect describes the emergence of Cherenkov radiation, when charged particles in a dielectric material travel faster than the local speed of light in this medium. The amount of produced Cherenkov light depends on the energy of the gamma-ray (higher gamma energy → larger air shower → more secondary electrons and positrons → more Cherenkov light).

2.2.3 Imaging Air Cherenkov Telescopes (IACTs)

The Cherenkov light follows a cone like shape, which has a radius of roughly 120 m at an altitude of ∼2000 m above sea level. So called Imaging Air Cherenkov Telescopes (IACTs) are collecting this Cherekov light, to draw conclusions about the gamma-ray which induced the air shower and the Cherenkov cone. Figure 4 shows the general idea of an IACT, which is hit by Cherenkov light from an air shower, and what the camera of the telescope sees.

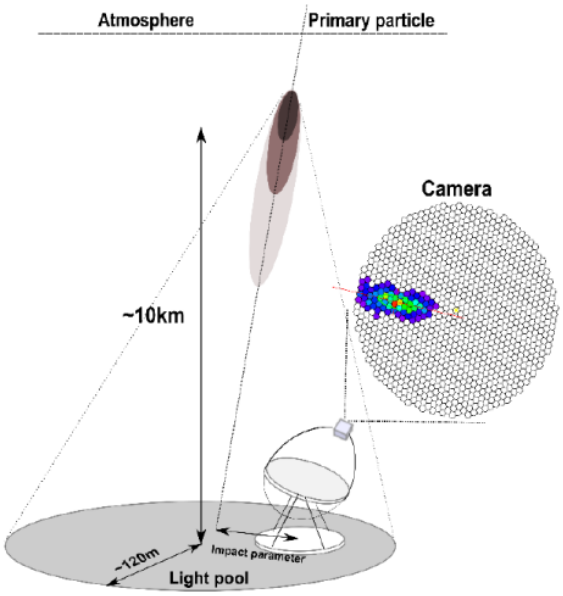

Figure 4: Principle of an IACT hit by a Cherenkov light cone [7]

2.2.4 The High Energy Stereoscopic System (H.E.S.S.)

One of the best currently operating gamma-ray detecting systems is H.E.S.S., which consists out of five IACTs located in Namibia, Africa (see Figure 5). Having an array of telescopes increases the sensitivity. H.E.S.S. investigates gamma-rays from ∼50 GeV to ∼100 TeV. The first four telescopes started their operation in December 2003. The fifth telescope, much larger than the first four, started collecting data in July 2012 and lowered the energy threshold, because of the larger mirror area. Until today H.E.S.S. found numerous new galactic and extragalactic sources of gamma-rays and was awarded several highly acknowledged prices. [8], [10]

Figure 5: The five telescopes of H.E.S.S. [9]

3 Cherenkov Telescope Array (CTA)

The next generation of IACTs will be the 'Cherenkov Telescope Array' (CTA), which is currently under development. CTA will cover gamma-rays with energies from 30 GeV to 300 TeV. There will be two arrays of telescopes, one in the northern hemisphere, on the canary island of La Palma, and one in the southern hemisphere, in Chile. The arrays will consist out of three different types of telescopes, large sized telescopes (LSTs), which will cover the low energy range, medium sized telescopes (MSTs) for energies between 100 GeV to 10 TeV, and small sized telescopes (SSTs) to cover the very-high energy range up to 300 TeV. The southern array will contain all three sizes of telescopes, while the northern array will only contain LSTs and MSTs. A possible layout for the two arrays is shown in Figure 6. It can be seen, that the SSTs cover a large area, because the flux of gamma-rays decreases with increasing energies. [11]

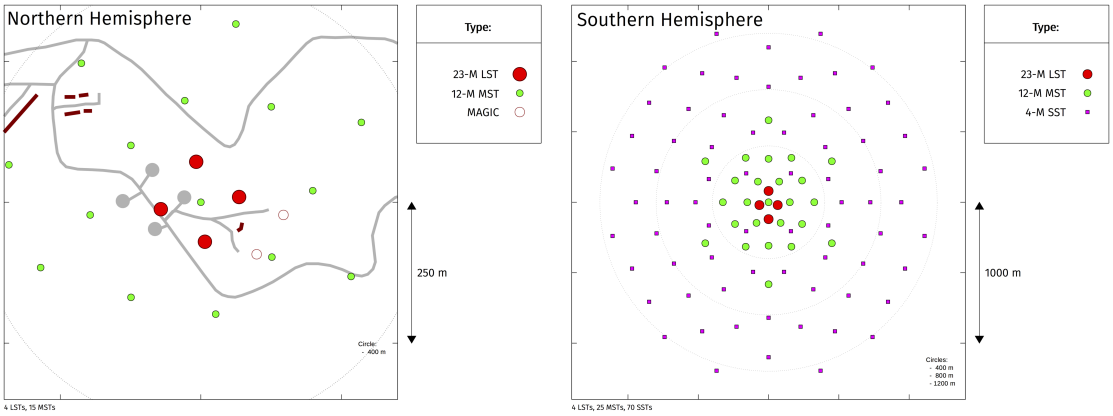

Figure 6: Proposed arrangement of the northern and southern array [11]

3.1 Large Sized Telescopes

Both arrays will have four LSTs in their center. A LST will have a parabolic mirror area of 400 m^2 with a diameter of 23 m. The LST needs to be very nimble to allow fast re-positioning, to observe for example gamma ray bursts, which last only a few seconds. How a LST will look like can be seen in Figure 7. In total it will be 45 m tall and will have a weight of 100 tons. [11]

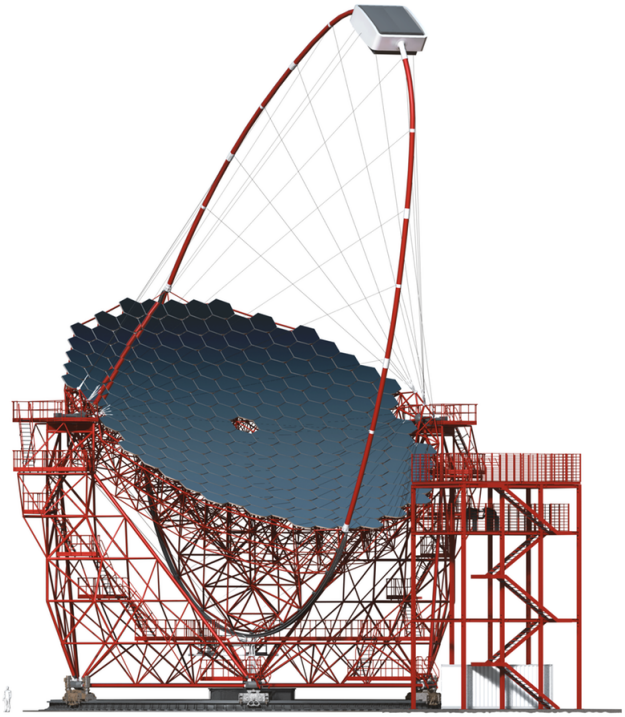

Figure 7: Illustration of the LST [11]

3.2 Medium Sized Telescopes

There will be 25 MSTs in the southern array and 15 in the northern. For the MSTs there are two proposed designs. The first one is a Davies-Cotton Telescope (DCT) with a reflecting diameter of 12 m. One DCT has been set up in Berlin (see Fig. 8a) and is currently being tested. [11]
The second design for a MST is a Schwarzschild-Couder Telescope (SCT) with a 9.7 m primary mirror area and a 5.4 m secondary mirror area (see Fig. 8b). At the moment a SCT prototype is built in Tucson, Arizona, and will then undergo performing tests. [11]

(a) DCT prototype at Berlin

(b) Illustration of proposed SCT design

Figure 8: Two designs for the MSTs [11]

3.3 Small Sized Telescopes

The southern array of CTA will contain 70 SSTs, for which there are three possible designs. All three of them have a primary mirror area of about 4 m. The first design, the 'SST-1M' (Fig. 9a), is in general a scaled down version of the Davis-Cotton Telescope design for the MST.
The other two designs suggest a Schwarzschild-Couder setup with two reflective areas. The diameter of the second mirror area is 2 m for the 'SST-2M GCT[6]' (Fig. 9b), and 1.8 m in the case of the 'SST-2M ASTRI[7]' (Fig. 9c). [11]

[6] Gamma-ray Cherenkov Telescope
[7] Astrofisica con Specchi a Tecnologia Replicante Italiana

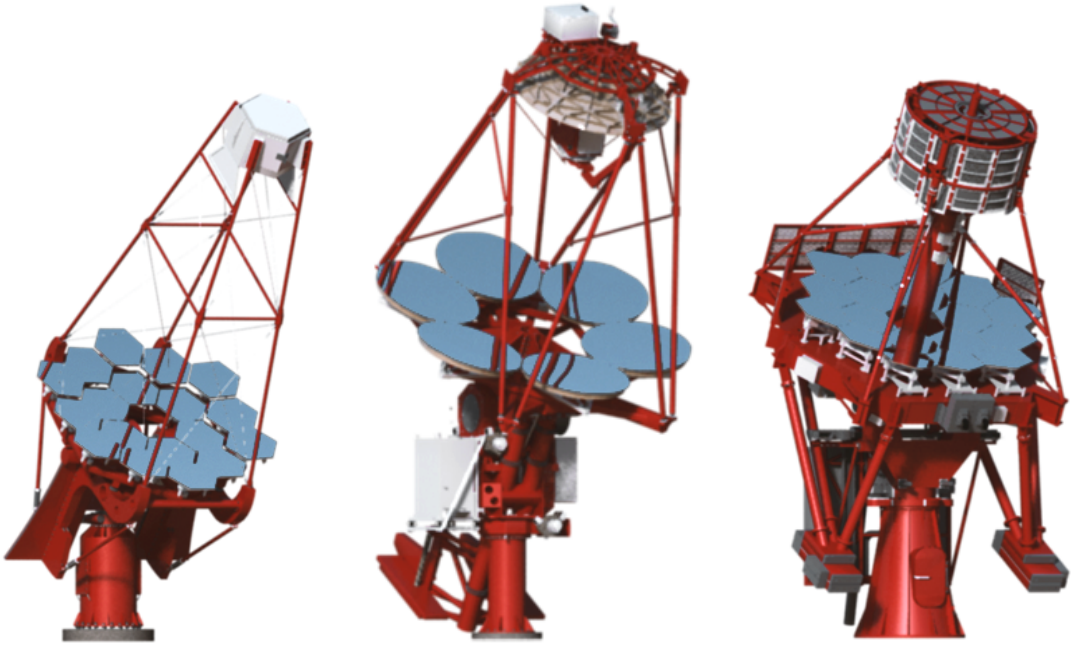

(a) SST-1M **(b)** SST-2M GCT **(c)** SST-2M ASTRI

Figure 9: Three designs for the SSTs [11]

3.4 Compact High Energy Camera (CHEC)

The Compact High Energy Camera (CHEC) is a possible design for the cameras of the SST-2M GCT. It will have a diameter of ∼0.4 m. CHEC is able to detect Cherenkov flashes from a few to a hundred of nanoseconds and will have a field of view of above 8°. In total the camera will have 2048 pixel with a size of $\sim 6 \times 6$ mm^2.
The camera will contain the following parts ([12], [13], [14], [15]):

- **Photosensors -** There are two generations of CHEC. The first generation, CHEC-M, uses Multi-anode photomultipliers (MAPMs), while the second generation, CHEC-S (see Fig. 10), will use Silicon photomultipliers (SiPMs).
- **Preamplifiers -** Amplify and shape the detected signal for the front-end electronics Target Modules.
- **Target Modules/Front-end electronics (FEE) modules -** 32 Target Modules with 64 channels providing triggering and digitization.
- **Backplane -** The 32 Target Modules are plugged into the backplane printed circuit board (PCB), which routes the data to one/two data acquisition board(s) (DACQ).
- **DACQ-Board(s) -** CHEC-M uses two DACQ boards with four 1Gbps links, while CHEC-S only uses one board, providing a data flow of 10Gbps. The DACQ board(s) send(s) the data to a PC and control(s) the backplane and the peripherals.

- **LED-Flashers -** In each corner of the camera there will be one LED-Flasher to calibrate the camera.
- **Cooling -** The camera is cooled via a chiller unit and internal fans, to keep the temperature stable.
- **Lid -** Protect the photosensors from damage.
- **Peripherals Board -** Controls the Lid, Cooling system and LED-Flashers.

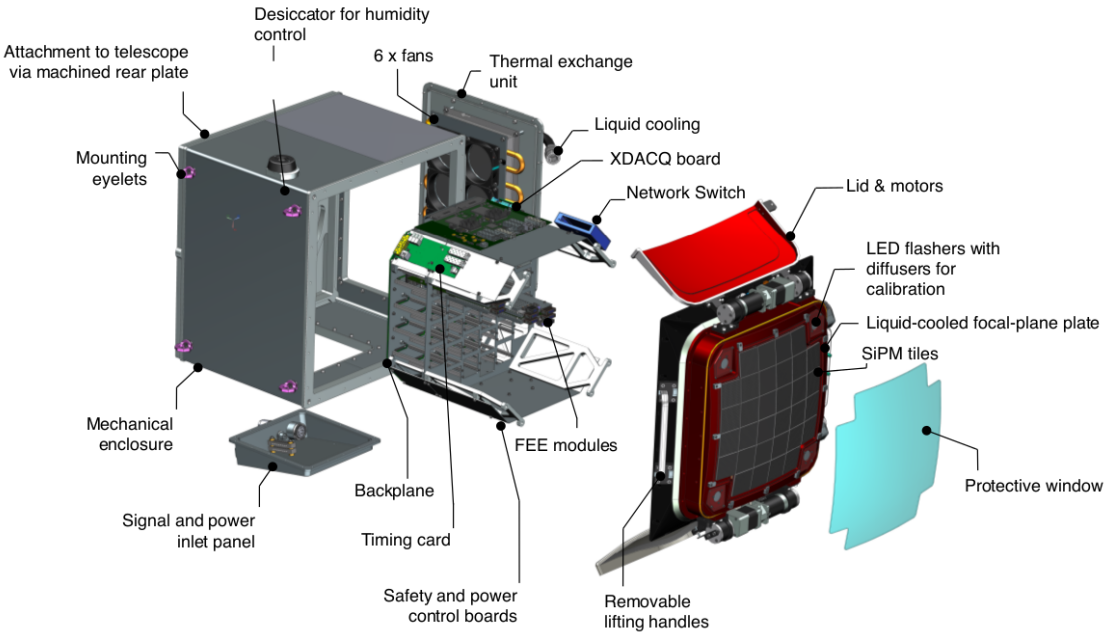

Figure 10: Illustration of the CHEC-S and its components [15]

A prototype of of a CHEC-M has been installed at the Observatoire de Paris-Meudon in 2015 and already measured the first Cherenkov light. [13]
The components of the CHEC-S, like the Target C Module in this thesis, are currently undergoing test.

4 Target C Module

A picture of a TC module and its components can be seen in Figure 11. The purpose of the module is to do the sampling, first-level triggering and digitization of the incoming signals. A signal from the SiPM firstly passes a pre-amplifier. Via shielded ribbon cables it gets sent into the module. Since the SiPM sends large pulses of about 30 ns, what could lead to an overlap of several pulses, they get shaped (see Figure 12) in front of the Target ASICs, which do the triggering (T5TEA) and sampling (Target C). Previous

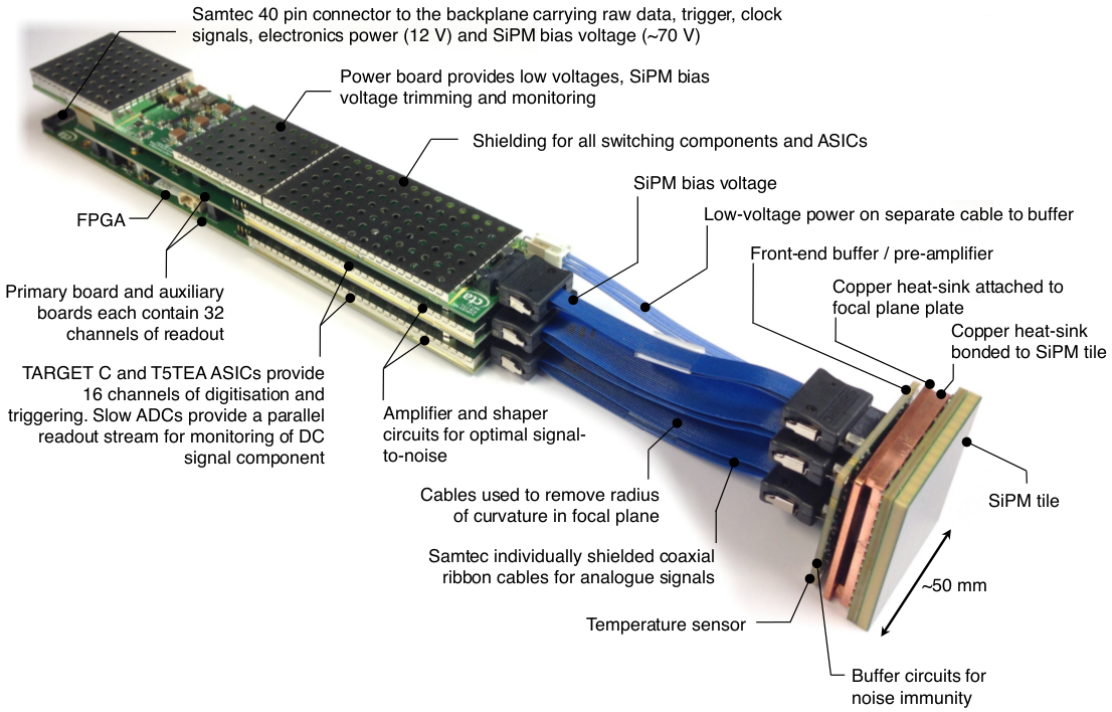

Figure 11: Picture of the Target C Module connected to a SiPM with 64 pixels [15]

generations of Target used only one ASIC for triggering and digitization. In order to reduce the noise-coupling between the triggering- and the digitization-path the TC Module uses two ASICs. One TC Module contains four T5TEA and TARGET C ASICs, each of them having 16 channels. So in total one module handles the signals of 64 pixels. A field-programmable gate array (FPGA) configures the ASICs of the module, reads out raw-data and buffers the data for the output. [15], [17]

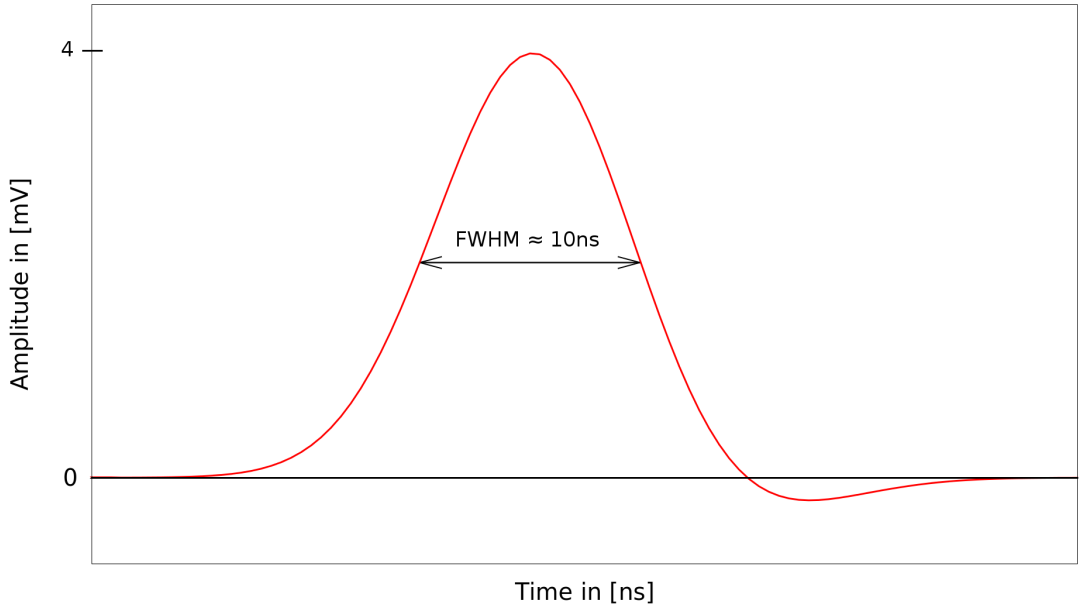

Figure 12: Shaped signal of a single photon which goes into the ASICs with a FWHM of ∼10ns

4.0.1 Target C

The sampling and storage of signals is done by switched-capacitor arrays (SCAs). Sampling uses 64 capacitors which are separated into two blocks of 32 respectively. These blocks work in a ping-pong mode, which means that one block samples data, while the other block buffers the data into the storage array.
The storage array consists out of 16,348 cells per channel. One cell is able to buffer ∼ 1 ns, so in total Target C has a buffer depth of ∼16 µs
Digitization is done with Wilkinson ADCs. They pass a voltage ramp to every channel. Simultaneously a 12 bit counter is counting. When the ramp crosses the analogue signal the corresponding counts are stored in the shift register. The Wilkinson ADCs have a digitization clock speed of 500 MHz.
Since digitization is only needed when an interesting event occurs, it is requested by the FPGA when it gets a signal from a higher level trigger logic. [17], [20], [21]

4.0.2 T5TEA

T5TEA has 16 channels. These are grouped together in triggergroups or superpixels of four channels, by building the analog sum. Via a comparator the threshold is compared to the signal of a triggergroup. When the signal crosses the threshold we get a trigger and a signal is sent to the FPGA, which can send a signal to TARGET C to start digitization. In T5TEA there a several parameters which can be adapted. The ones that were varied in the following measurements are ([17], [18]):

- **Thresh** controls the threshold which needs to be crossed to get a trigger. This is done by setting a reference voltage to a comparator.
- **Vped** can be adapted for every channel respectively and controls the offset of a single channel.
- **PMTref4** is an offset of the summed up signal for the four channels of a triggergroup (superpixel) and shifts the signal closer or further away from the threshold.

All parameters are controlled by a 12 bit DAC (digital to analog converter). Hence they can be varied between 0 and 4095 DAC-counts.
The principle of a triggergroup and what Vped and PMTref4 do, can be seen in Figure 13.

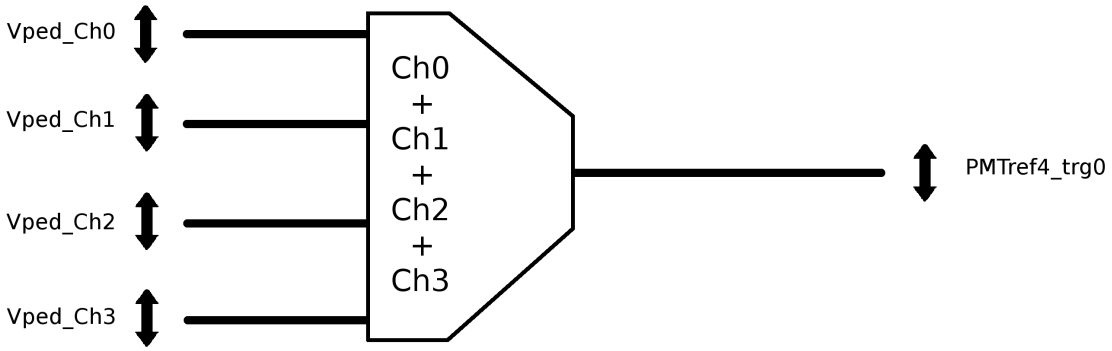

Figure 13: Illustration of how the four channels (here: 0,1,2,3) are put together in a triggergroup (here: 0) and what the parameters Vped and PMTref4 do

5 Parameter-Scans with the Target C Module

For all 64 channels of the TC module parameter scans have been done. Their aim was to check on which pulse amplitudes ($\widehat{=}$ amount of Cherenkov light) they are able to trigger and what their noise is. These measurements are then compared to earlier measurements, which have been done with an evaluation board, only consisting out of T5TEA, TARGET C and components to control them (e.g. the FPGA).
Furthermore, the spread between the channels is examined. For the final camera there will be look-up tables with PMTref4-Thresh pairs corresponding to different thresholds like

e.g. 40 mV ($\widehat{=}$ 10 photoelectrons). Since all channel should trigger on the same threshold the variations between the channels should not be too big ($< 5\%$). [21]

5.1 Measurement-Setup of the Scans

The setup can be seen in Figure 14. A waveform generator simulates pulses of a SiPM. The signal then goes into a splitterboard which distributes it to the input channels of the TC module. One splitterboard can handle 32 channels ($\widehat{=}$ two ASICs), so the final test setup will contain two splitterboards per module. The TC module triggers (T5TEA) and digitizes (Target C) the signal and via a standalone adapter the data gets send to a PC. Also two power supply units (PSUs) are needed to power the splitterboard and the module.

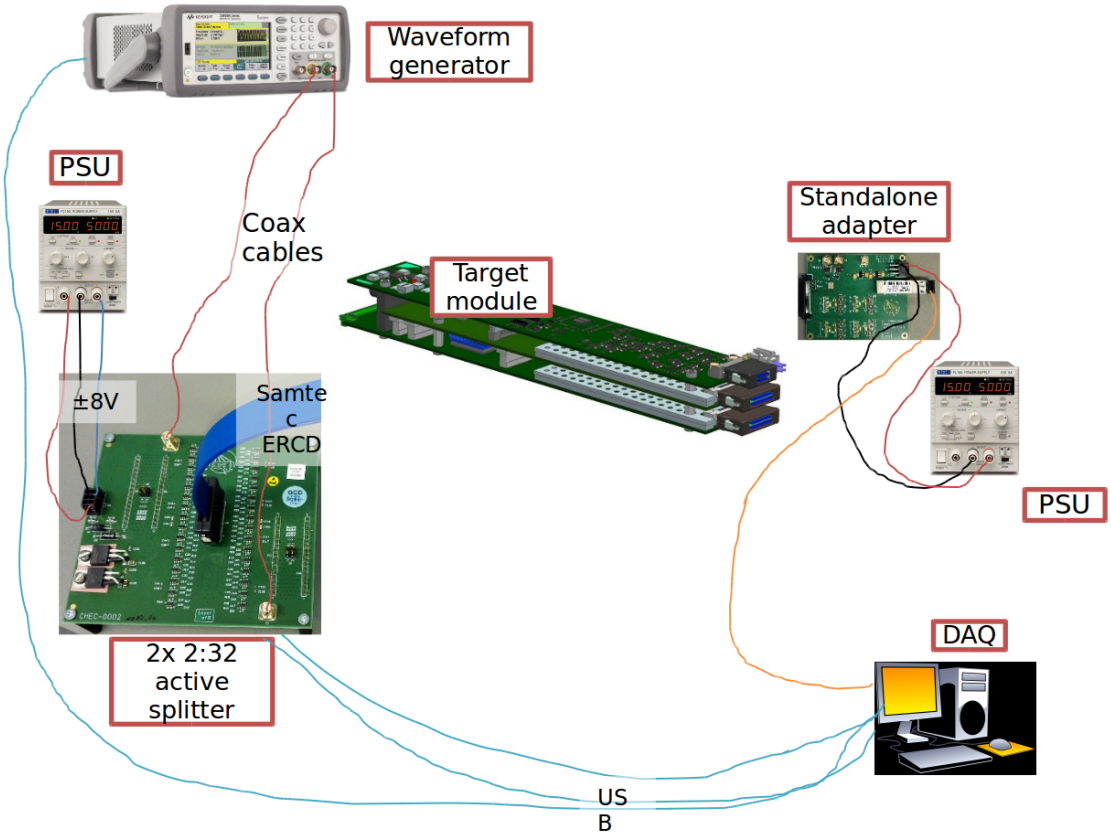

Figure 14: Setup of the parameter-scans with all necessary instruments [16]

5.2 Choosing the Parameter-Values of the Scan

The following parameter-values were chosen for the scans:

Thresh_beg	Thresh_end	Thresh_steps	PMTref4_steps	Voltage_min	Voltage_max	Vped
1950	2050	10	10	0 mV	100 mV	1100

Table 1: Settings of the PMTref4-Thresh scan for one channel (all values are given in DAC counts except for the voltages)

The Thresh range of 1950 - 2050 DAC counts was chosen, because in this range the scans behave roughly linear, as earlier measurements with the evaluation board showed (see the plot in Fig. 15).

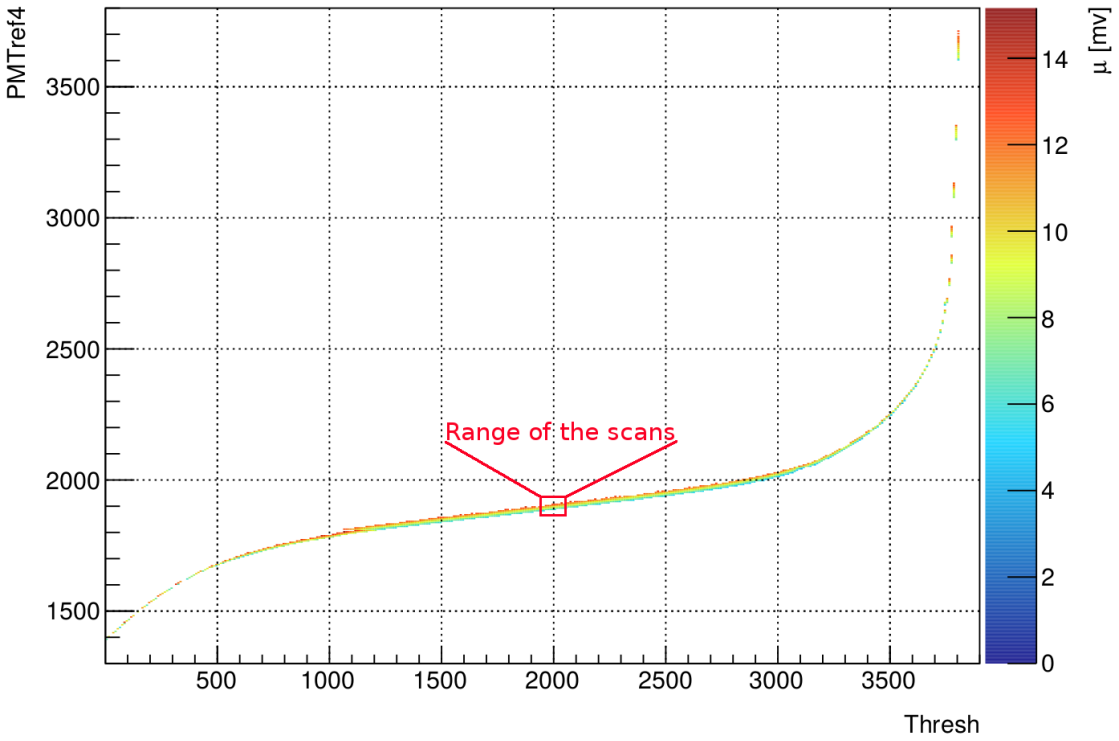

Figure 15: PMTref4-Thresh scan over the whole parameter range for channel 0 with a color coded μ-value [19, page 27] (what the μ-value describes will be explained in Section 5.4)

The range of PMTref4 is variable as can be seen later (Section 5.5), so only the step-size needs to be adapted.
Thresh and PMTref4 steps of 10 make a rather rough parameter scan, which is fine for the aims of the measurements and make the scan not to last too long (∼2h per channel).
The voltage range from 0 mV to 100 mV corresponds to ∼ 0 to 25 photoelectrons.
All Vpeds were chosen to be 1100 DAC counts, because this value gives a good transfer function and simultaneously offers a good charge resolution. [21]
(for further informations on the transfer function and charge resolution see [17])

5.3 Finding the Baseline

Then the first Thresh-value is adjusted (in this case 1950), the PMTref4-value is slowly increased, starting at 900, to find the baseline. How this works can be seen in Figure 16. In the beginning the signal (= Vped + PMTref4 + Noise) is below the threshold and no triggers are measured. When PMTref4 gets increased there is a point when the noise crosses the threshold for the first time and a few triggers are measured. Further increasing of PMTref4 creates more and more triggers until the signal is above the threshold and the number of triggers decreases until finally the noise does not cross the threshold anymore and no more triggers are detected.
That is how the peak in Figure 16 occurs. The baseline is where the peak has its maximum. The first PMTref4-value of the scan is the value where no more triggers are measured after the peak.

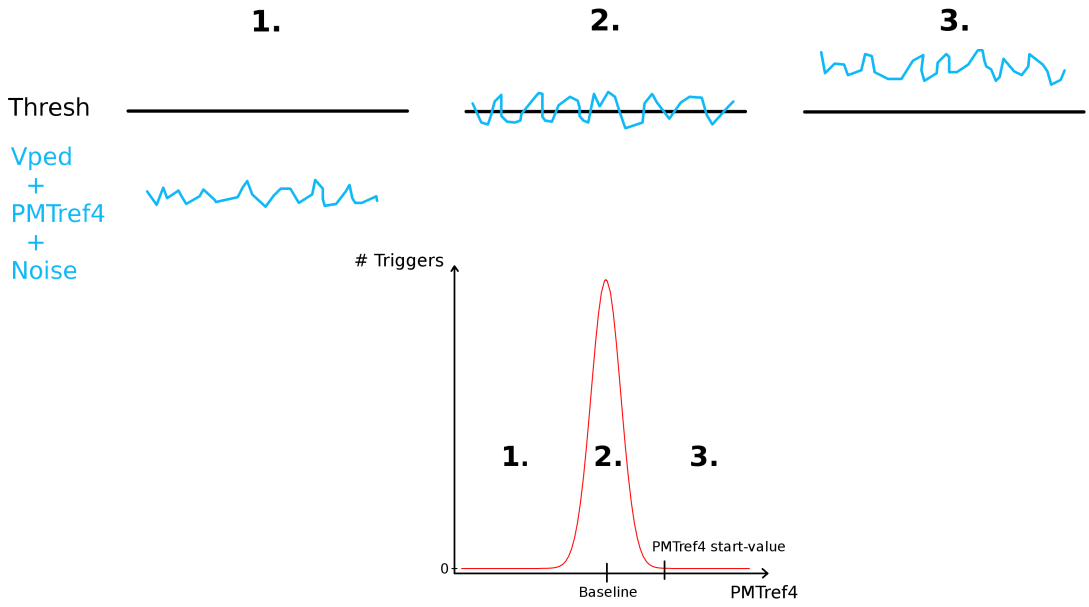

Figure 16: Illustration of how the baseline is searched

5.4 The Scan

Then the waveform generator is turned on and simulates signals from a SiPM (see Fig. 17), which get shaped and inverted, before they go into T5TEA (see Fig. 12). The first step of amplification in T5TEA includes another inversion.

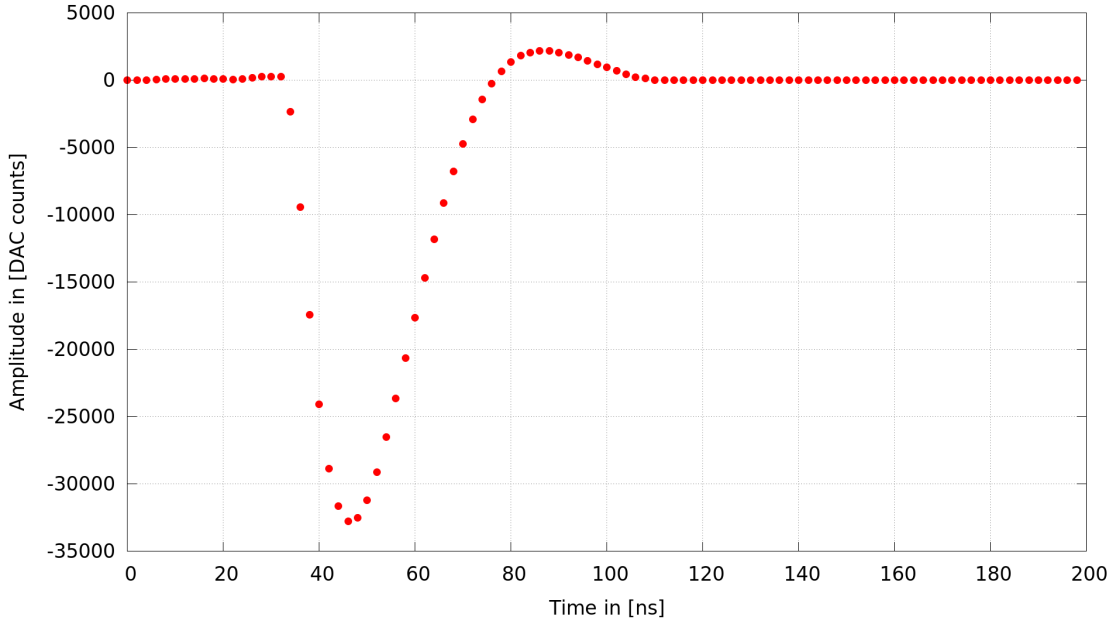

Figure 17: Simulated pulse of a SiPM generated by the wave-generator

The pulses are generated with a frequency of 1 kHz .
Then the amplitude of the pulse is increased until the trigger-efficiency (ϵ) reaches 100%. The trigger-efficiency describes the ratio between the number of measured triggers (N_{meas}) and the number of expected triggers (N_{exp}):

$$\epsilon = \frac{N_{meas}}{N_{exp}}$$

Since the time of the measurement is 100 ms and the frequency of the pulses is 1 kHz, the number of expected triggers is 100.
The trigger-efficiency, depending on the amplitude of the pulse, follows a Gaussian error function:

$$f(A;\mu,\sigma) = \frac{1}{2}(1 + \mathrm{erf}(\frac{A-\mu}{\sqrt{2}\sigma}))$$

So the function $f(A;\mu,\sigma)$ is fitted into the data to determine the μ-value, which describes the amplitude where the trigger-efficiency is at 50%, and the σ-value, which describes the noise of the threshold ($\widehat{=}$ μ-value). This can be seen in Figure 18.

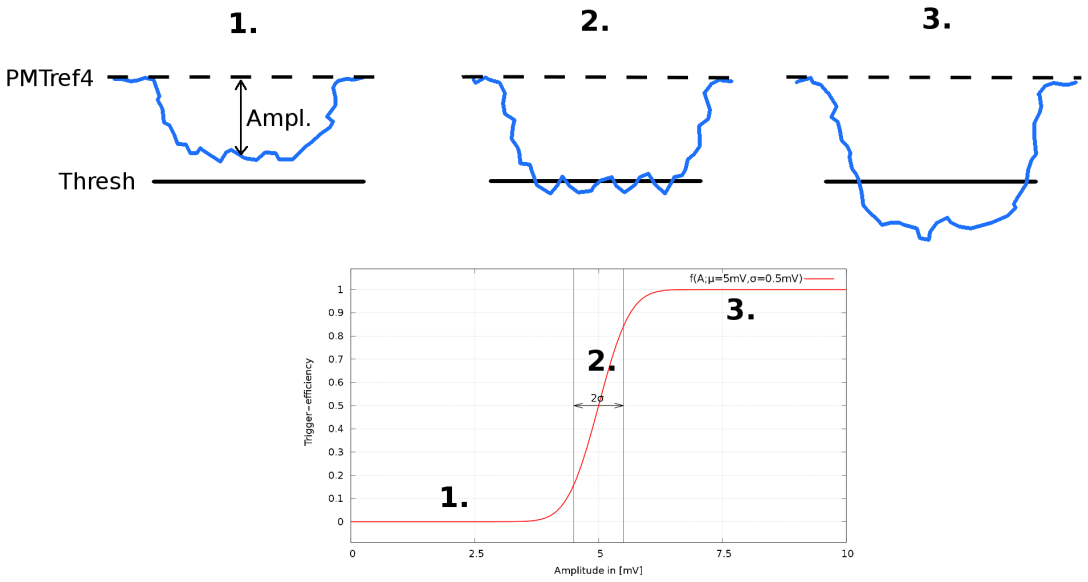

Figure 18: Illustration of how the error function evolves with increasing voltages for one PMTref4-Thresh pair (this error function has the values $\mu = 5mV$ and $\sigma = 0.5mV$)

Then the PMTref4-value is set to the next value (= PMTref4 + PMTref4_steps) and μ and σ are determined for this PMTref4-Thresh pair.
This continues until the maximum voltage of the pulse (100 mV) can not reach the threshold anymore, because PMTref4 is too high.
After this the next Thresh-value (= Thresh + Thresh_steps) is applied and the measurement starts again with the search for the baseline.

5.5 Plots of the PMTref4-Thresh scans

The measured data can be plotted in 2D plots with the Thresh-value on the x-axis, PMTref4 on the y-axis and μ or σ color coded. The Figures 19, 20 and 21 show these plots for the channels 0, 28 and 54 (plots of the other channels can be found in the appendix). All plots have roughly the same structure, being linear with a slight slope, what is expected, as earlier measurements over the whole parameter range showed (see Fig. 15). This means that no channel seems to have defects. What changes, is the location of the PMTref4-values. Channel 0 has values from 1850 to 2060 DAC counts, while channel 28 has values from 1880 to 2070 DAC counts. This will be further analysed in section 5.7. Besides the location of the PMTref4 area, the total range of PMTref4 also varies from channel to channel, with a minimum range of 160 DAC counts at channel 58, and a maximum range of 240 DAC counts at channel 19.

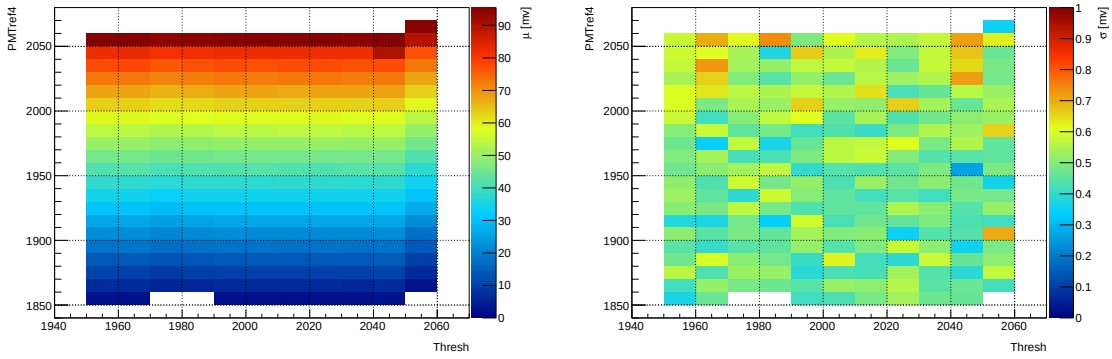

Figure 19: Mean (μ) and noise (σ) of channel 0

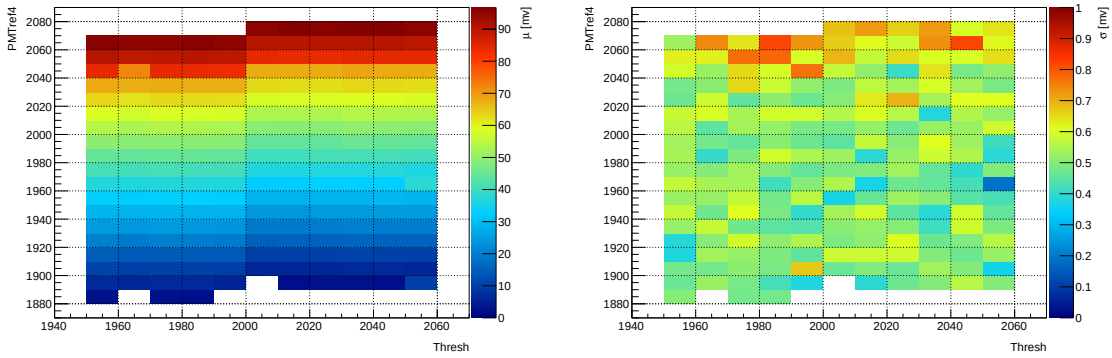

Figure 20: Mean (μ) and noise (σ) of channel 28

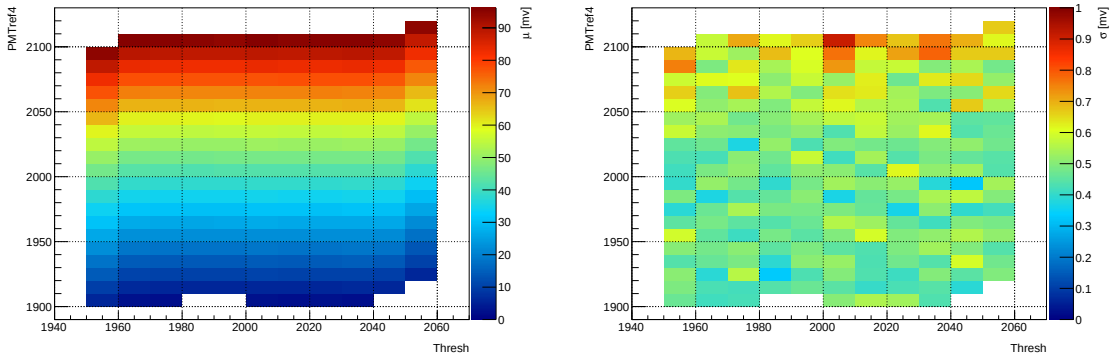

Figure 21: Mean (μ) and noise (σ) of channel 54

5.6 Lowest μ- and σ-values

One property we are interested in is the lowest achievable values of μ and σ. The lowest μ-value tells us at which input-voltage the module is still able to measure 50% of the expected triggers. The lowest σ-value tells us the lowest noise which is achievable. Since the measurements have been made with Thresh and PMTref4 steps of 10 the real lowest values might be even smaller. Figures 22 and 23 show these plots (the errorbars are the fitting errors of the Gaussian error function). The μ-values all lie between 2 and 3 mV, with a mean-value of (2.436 $\pm$ 0.020) mV. The σ-values lie between 0.2 and 0.5 mV with a mean of (0.338 $\pm$ 0.003) mV. Previous bachelor theses also did PMTref4-Thresh scans. They have been working with an evaluation board. A scan with channel 0 measured a lowest μ-value of (2.534 $\pm$ 0.011) mV [18], while the scans with the Target C module for channel 0 gave a lowest μ-value of (2.471 $\pm$ 0.026) mV. This means that the Target C module maybe brought a slight improvement, but the results of the evaluation board are also fine, since T5TEA is required to trigger on signals $\leq$ 10 mV with 50% efficiency. [21]

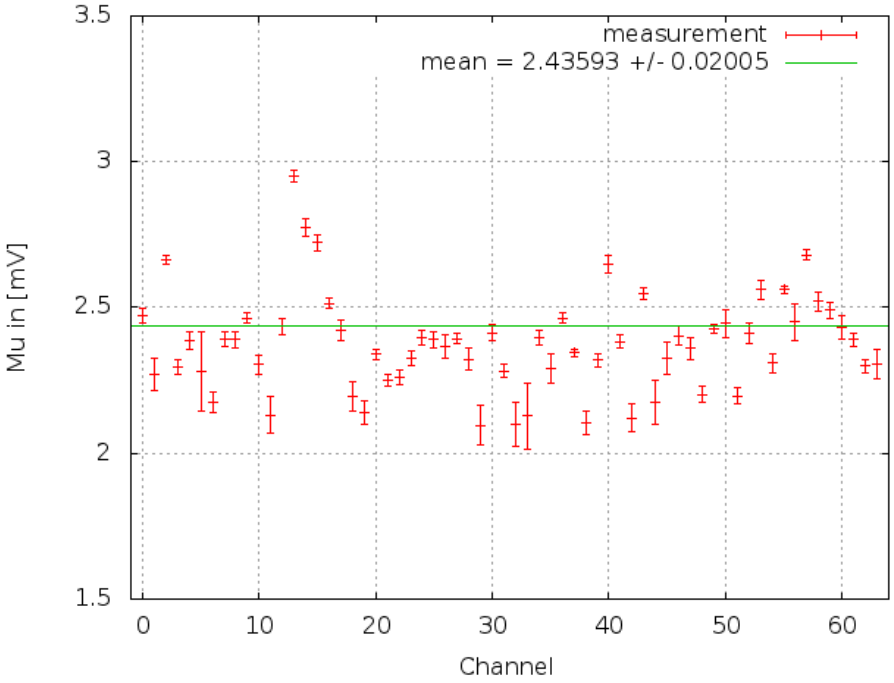

Figure 22: Lowest measured μ-values for all channels and their mean

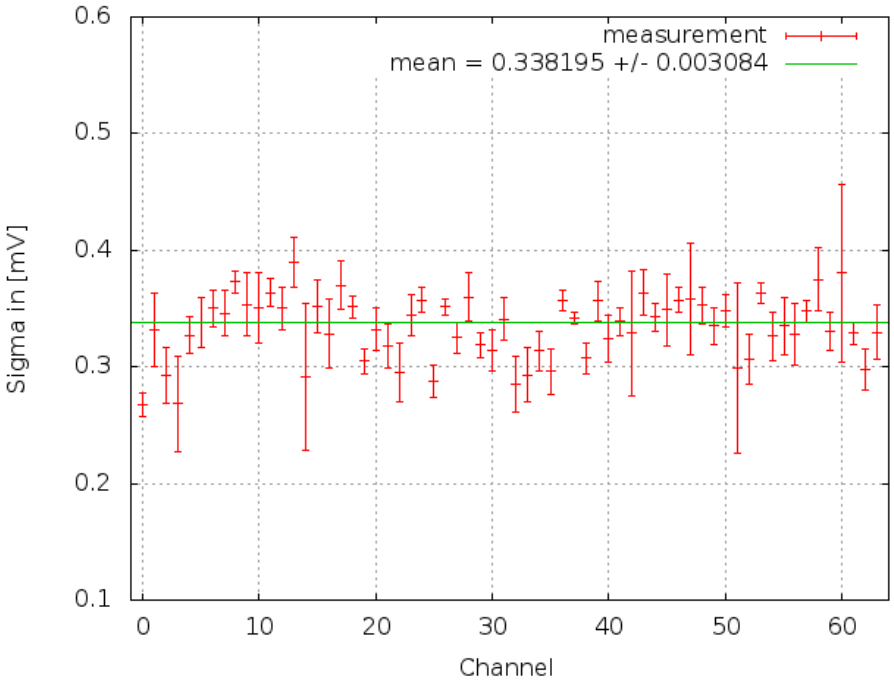

Figure 23: Lowest measured σ-values for all channels and their mean

5.7 Trigger on 20 mV

The final camera is going to trigger on a specific threshold (e.g. 10 mV,20 mV, 30 mV, ...), depending on the light conditions. This threshold is adapted by setting the corresponding PMTref4-Thresh pair. So it is interesting to see at which PMTref4-Thresh pairs the module triggers on a specific threshold (here: 20 mV) and how much they vary. This plot is shown in Figure 24 (for this and all following plots the Thresh-value was chosen to be 2000).

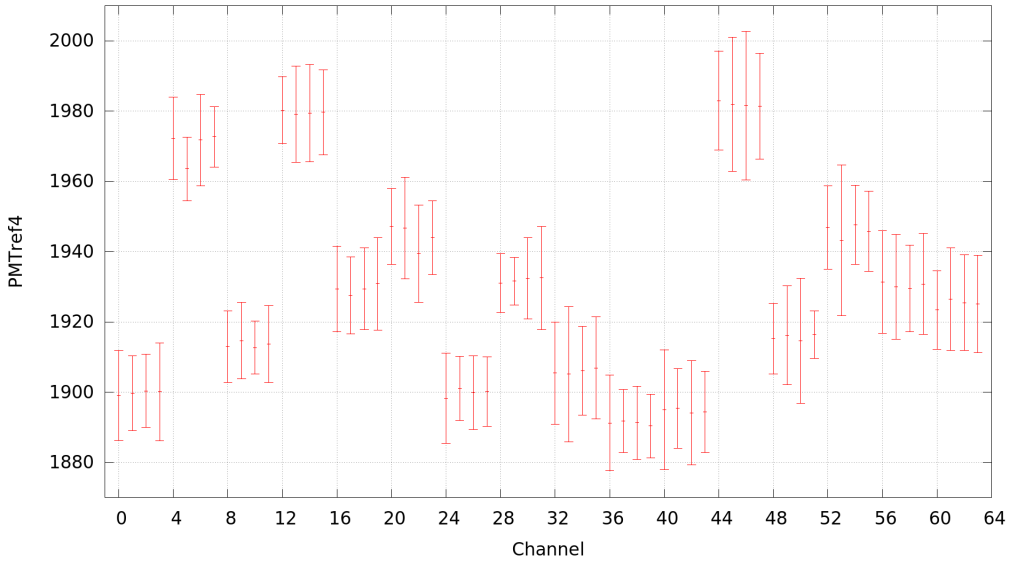

Figure 24: PMTref4-values at which the channels trigger on 20 mV with 50% efficiency at a Thresh-value of 2000

To create this plot it was necessary to extrapolate the PMTref4-values at which triggers of 20 mV are achieved, because it is unlikely to measure exactly a μ-value of 20 mV, especially with a large PMTref4 step-size of 10. How the parameter-scan results for channel 0 look like can be seen in the following table:

PMTref4	Thresh	μ	μ_err	σ	σ_err
1884	2000	14.2208	0.0214063	0.62095	0.0289041
1894	2000	18.0029	0.0135303	0.439883	0.0194257
1904	2000	21.9013	0.0127719	0.494975	0.0190182
1914	2000	25.8065	0.00881007	0.429304	0.0133861

Table 2: Excerpt of the PMTref4-Thresh scan data of channel 0

The extrapolation has been done by assuming a linear correlation between PMTref4 and μ in this small range. For channel 0 this yields a PMTref4-value of 1899.12 ± 12.80 for 20 mV. Here and in the following plots, the errors were calculated with Gaussian error propagation of the fitting errors.
The plot shows that there are variations between the triggergroups, but at least the values in every triggergroup roughly lay in the same area (this will be further analysed in the next section 5.8). This behaviour is needed, because PMTref4 only adapts the summed up signal of a triggergroup. If the variations between the single channels of one triggergroup would be too big, the channels would trigger on different μ-values within one triggergroup.

5.8 Deviation from triggergroup-mean

The next step is to check how big the variations in every triggergroup are. For this plot, PMTref4 was fixed to the value which is closest to 20 mV in the data of the first channel of each triggergroup (e.g. 1894 for the values of the Table 2 above for channel 0). For the other three channels μ was extrapolated for this fixed PMTref4-value. Then the mean of the four μ-values and their deviation from the mean was calculated. Figure 25 shows this plot.

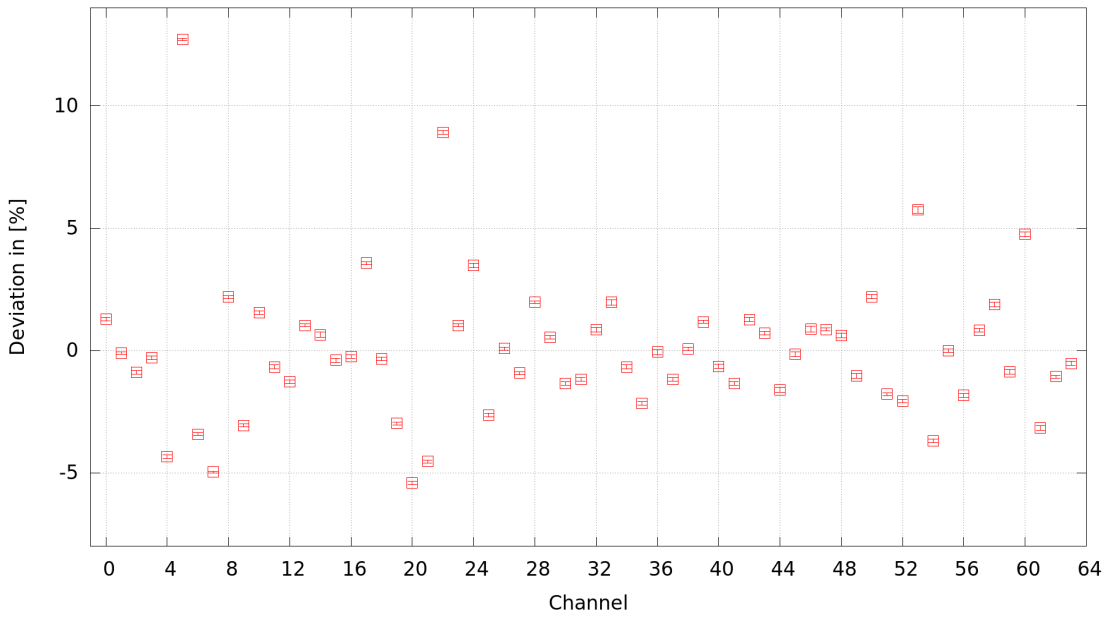

Figure 25: Deviation from triggergroup-mean for fixed PMTref4 at Thresh=2000

As can be seen most triggergroups have deviations from their mean-value of less than 5%. However, a few channels show larger deviations. For example channel 5 has a deviation of almost 13% or channel 22 has a deviation of $\sim$9%. Monte Carlo simulations including the

SiPM, the preamplifier and the Target C module gave deviations of less then 10%, so the Target C module was given a budget of 5%. [21]

5.9 Deviation from triggergroup-mean with Vped-adaptations

The offset of the single channels can be adapted with the Vped parameter. During the so far done measurements Vped has been set by default to 1100 DAC counts for every channel. Since there are large deviations in some channels we need more specific Vped-settings. This has been done by setting Vped of channel 0 to 1100 DAC counts as a reference value. Then the Vped-values of the other channels are varied until the same voltage, as in channel 0, is measured. Here the voltage was measured after the shaper of the module and therefore directly before T5TEA.
So far, this has been done for ASIC 0 and ASIC 1. The adapted Vped-values (in DAC counts) can be seen in the following table:

Asic 0		**Asic 1**	
Vped_0	1100	Vped_16	1110
Vped_1	1103	Vped_17	1096
Vped_2	1088	Vped_18	1090
Vped_3	1105	Vped_19	1097
Vped_4	1082	Vped_20	1103
Vped_5	1107	Vped_21	1082
Vped_6	1104	Vped_22	1071
Vped_7	1103	Vped_23	1088
Vped_8	1086	Vped_24	1098
Vped_9	1100	Vped_25	1095
Vped_10	1099	Vped_26	1109
Vped_11	1101	Vped_27	1093
Vped_12	1097	Vped_28	1091
Vped_13	1094	Vped_29	1075
Vped_14	1108	Vped_30	1078
Vped_15	1079	Vped_31	1100

Table 3: Adapted Vped-settings for the ASICs 0 and 1

With these values new PMTref4-Thresh scans were made for the triggergroups 1 (channel 4-7) and 5 (channel 20-23), because these two triggergroups showed the largest deviation from their mean-value (see Fig. 25). For the new scans also plots, which show the deviation of the triggergroup mean-value, were created. This was done similarly as explained in Section 5.8.
Here, plots for mean voltages of ∼10 mV, 20 mV and 80 mV were made, to cover the whole voltage range. They are then compared to the previous results without Vped-adaptations, to check whether the performance gets better. These plots can be seen in the Figures 26, 27 and 28. For all voltages the deviations get smaller with the tuned Vped-settings. What can also be seen is that the deviation decreases with increasing voltage, which is obvious, because the deviation in [%] is calculated with the following formula:

$$dev = (\frac{\mu}{mean} - 1) * 100$$

This means that the ratio $\frac{\mu}{mean}$ decreases with increasing voltages, if the absolute deviation at different voltages stays constant.
For all voltages the deviations with the adapted Vped-settings lie within 5%, except for channel 5 at 10 mV which has a deviation of (6.02 ± 0.13) %. If this behaviour is also observed in other modules than this has to be accepted, because then the modules can not perform better. If the other modules have smaller deviations, this module can be sorted out, because of not achieving the 5% requirement.

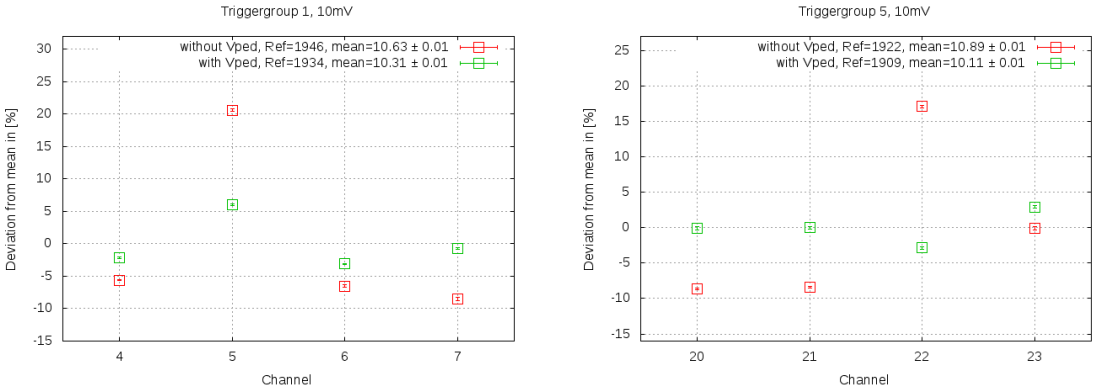

Figure 26: Deviation from triggergroup-mean at ∼10 mV with and without Vped-adaptations

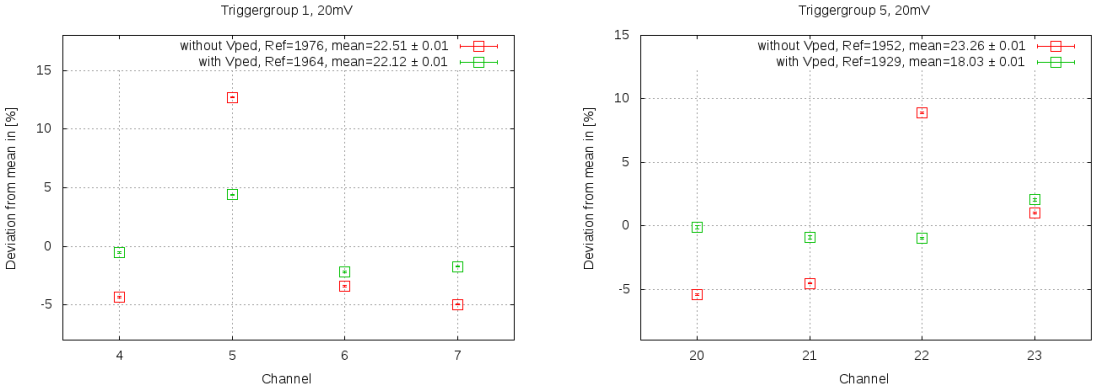

Figure 27: Deviation from triggergroup-mean at ∼20 mV with and without Vped-adaptations

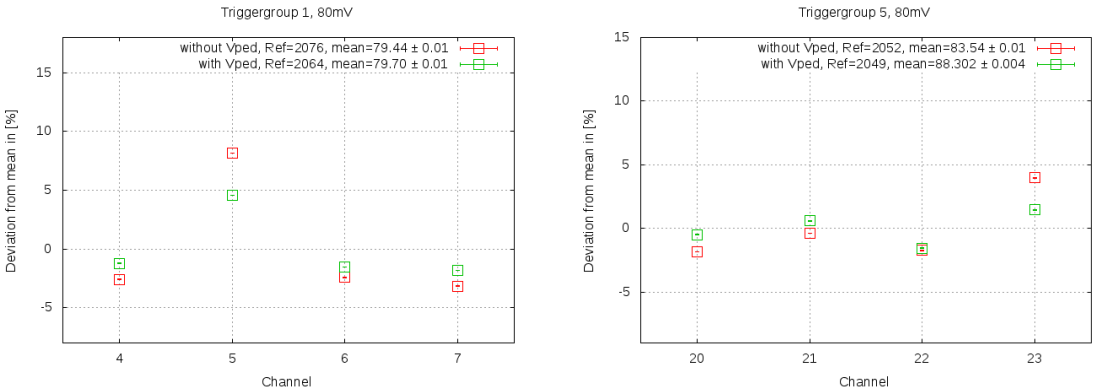

Figure 28: Deviation from triggergroup-mean at ∼80 mV with and without Vped-adaptations

6 Conclusion

Summarized, the Target C Module with the ASICs T5TEA and Target C performs at least as good as the evaluation board, which only contained T5TEA, Target C and the FPGA. PMTref4-Thresh scans measured lowest μ-values for every channel between 2 and 3 mV with a mean of (2.436 ± 0.020) mV. The lowest σ-values lie between 0.2 and 0.5 mV with a mean of (0.338 ± 0.003) mV. Since the final camera is required to trigger on values ≤ 10 mV with 50% efficiency the Target C Module perfectly meets this requirement.
The values of PMTref4 at a Thresh of 2000, where the module triggers on 20 mV vary (Fig. 24), but the variations in each triggergroup are rather small.
To check how much the triggergroups vary from their mean μ-value at a Thresh of 2000 and a fixed PMTref4-value the plot in Figure 5.8 was created. Most of the channels do not vary more than 5%, but a few channels have larger deviations (e.g. channel 5 or channel 22). To get rid of these large deviations the Vped-values have been adapted, which control the offset of every channel. With these tuned Vped-settings new PMTref4-Thresh scans for triggergroup 1 and 5 have been made, to see whether the deviation gets smaller. Over the whole voltage range ($\sim$10 mV, 20 mV and 80 mV) the deviations decreased notably and are smaller than 5%, except for channel 5 at 10 mV, where the deviation is still about 6%.

7 Outlook

The next step in the commissioning of CHEC-S is to connect the Target C Module to the backplane. With tuned Vped-settings PMTref4-Thresh scans need to be done. In this measurements the μ-values should not vary more than a few percent. If this is achieved, look-up tables can be created. They should contain PMTref4-Thresh pairs for certain μ-values. So if the module should trigger on a certain voltage (e.g. 10 mV) the corresponding PMTref4-Thresh values in the look-up table can be adapted.
Aside from that, a lot more tests with the module must be performed. For example the sampling speed has to be checked and should not vary too much from the assumed 1 $\frac{GSa}{s}$ of Target C. Also the transfer-function needs to be measured. [16]
After all these tests have been done, the full camera chain with a SiPM, a preamplifier, the Target C Module and the backplane can be tested.
It is planned to install and test a full CHEC-S in a GCT prototype within this year. [20]

8 Appendix

8.1 Plots of the PMTref4-Thresh scans

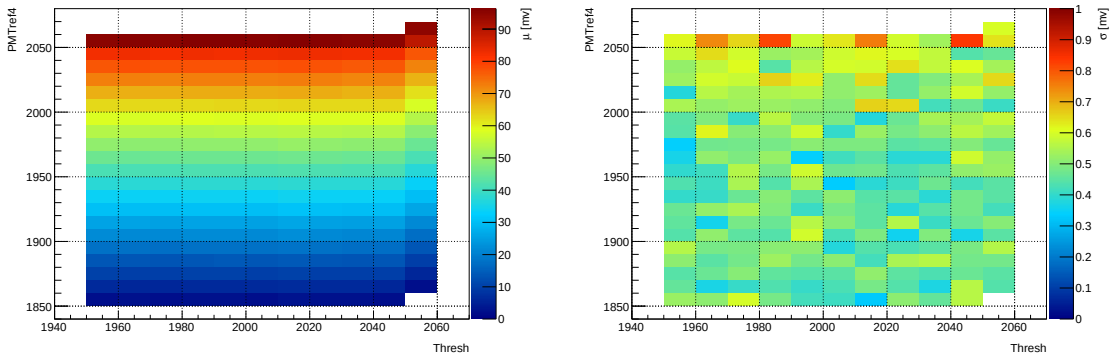

Figure 29: Mean (μ) and noise (σ) of channel 1

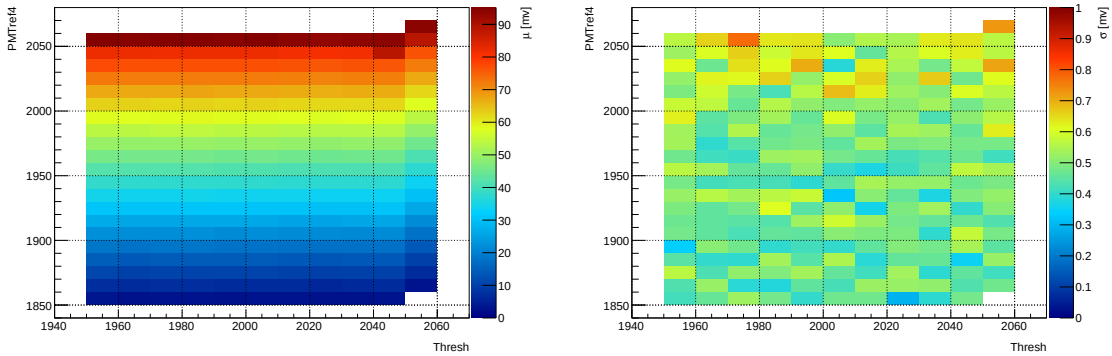

Figure 30: Mean (μ) and noise (σ) of channel 2

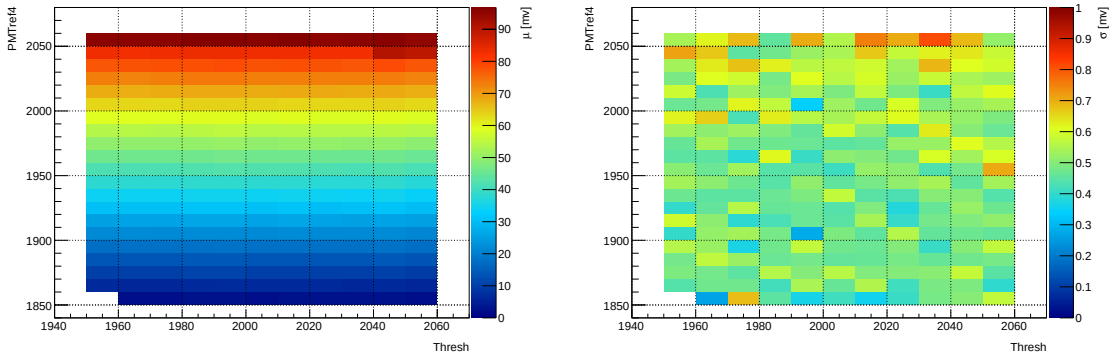

Figure 31: Mean (μ) and noise (σ) of channel 3

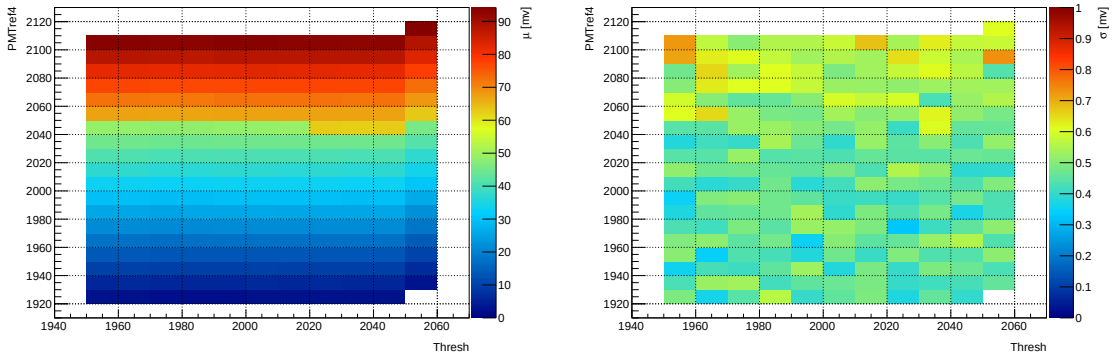

Figure 32: Mean (μ) and noise (σ) of channel 4

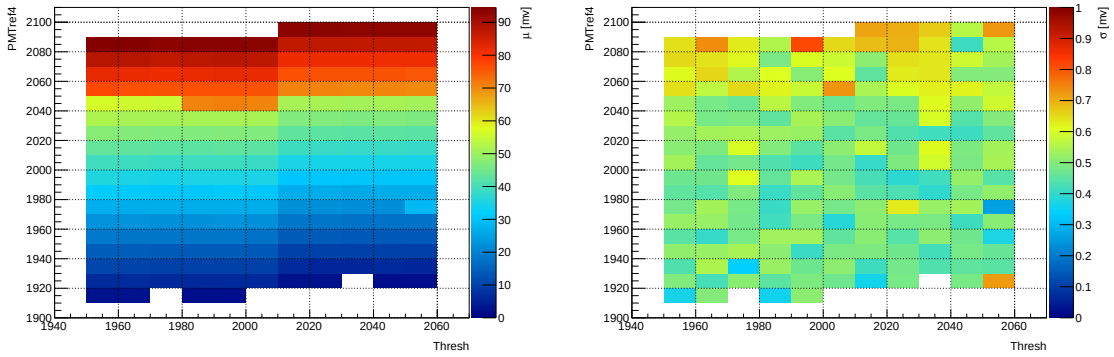

Figure 33: Mean (μ) and noise (σ) of channel 5

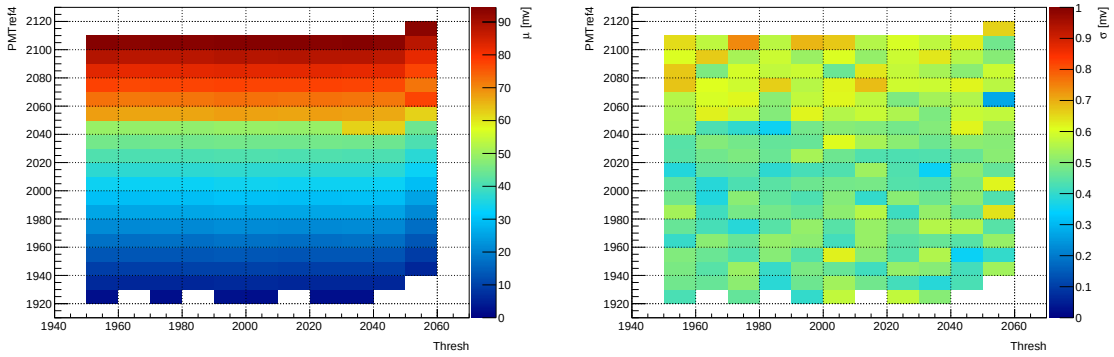

Figure 34: Mean (μ) and noise (σ) of channel 6

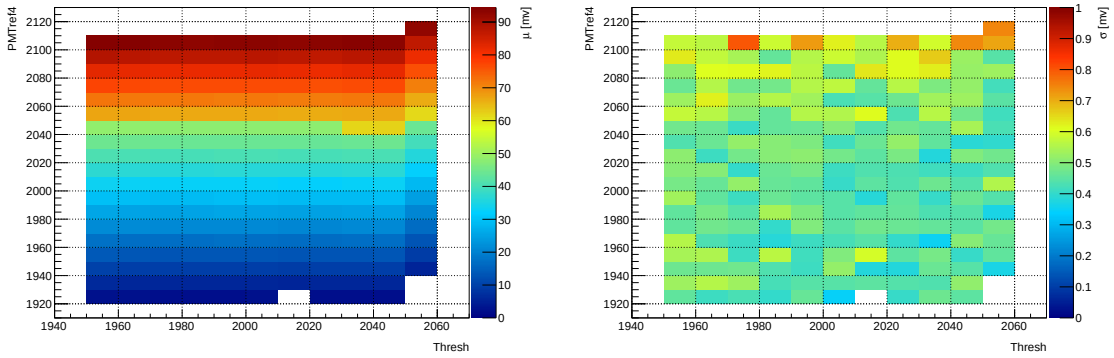

Figure 35: Mean (μ) and noise (σ) of channel 7

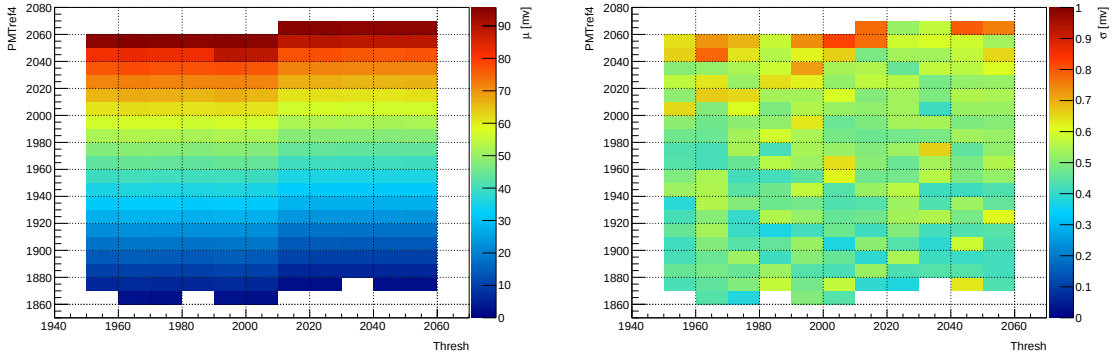

Figure 36: Mean (μ) and noise (σ) of channel 8

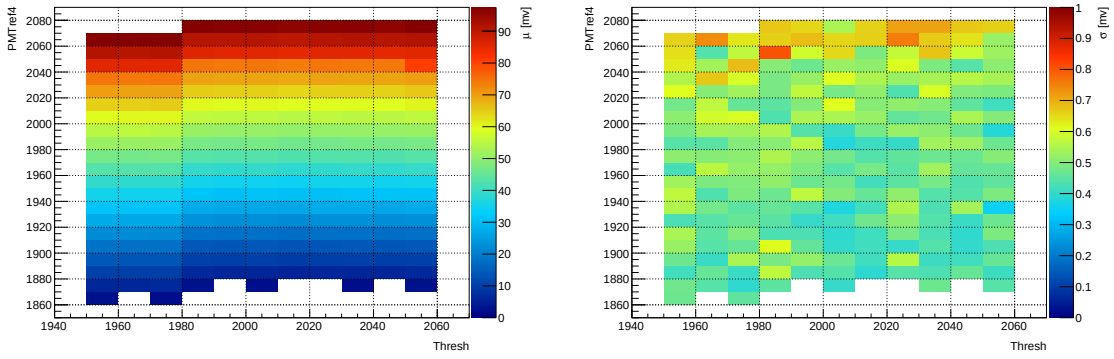

Figure 37: Mean (μ) and noise (σ) of channel 9

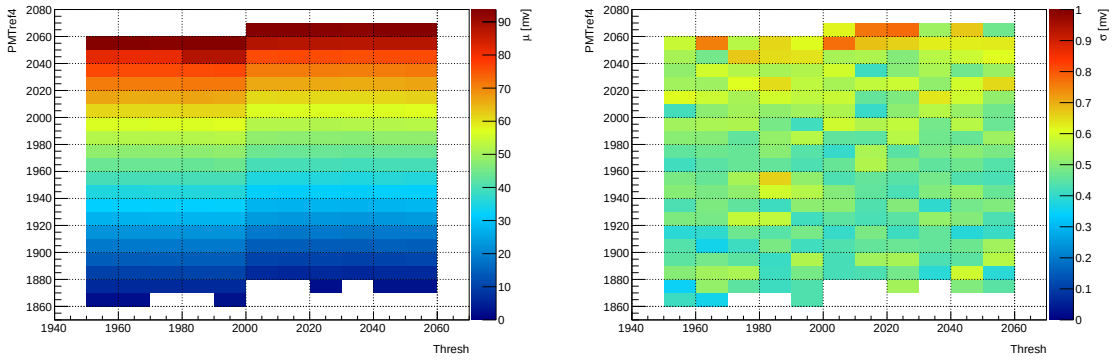

Figure 38: Mean (μ) and noise (σ) of channel 10

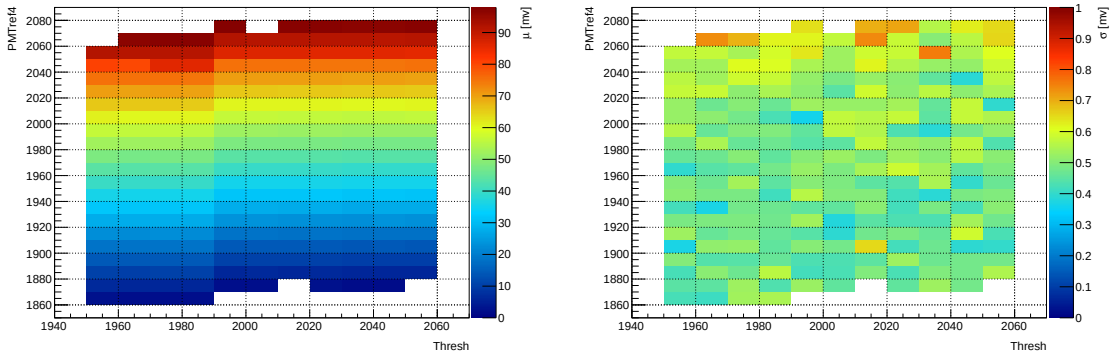

Figure 39: Mean (μ) and noise (σ) of channel 11

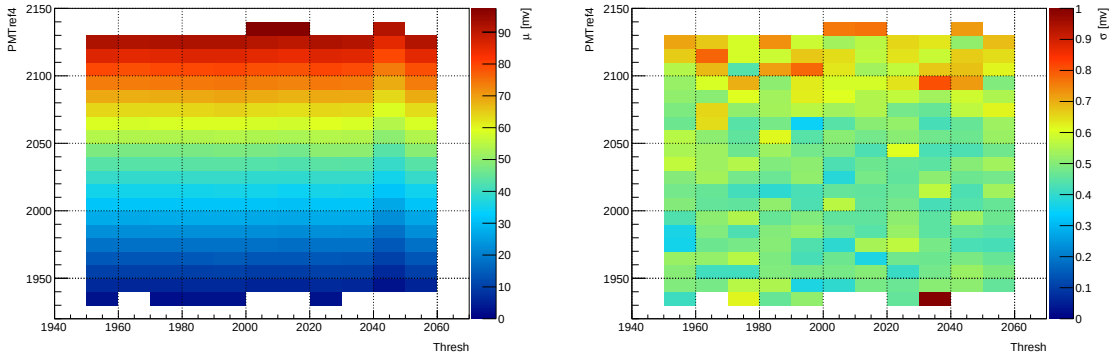

Figure 40: Mean (μ) and noise (σ) of channel 12

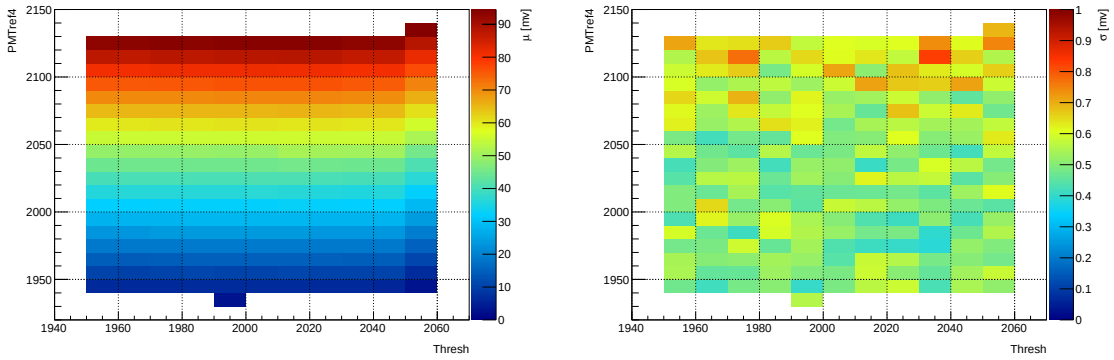

Figure 41: Mean (μ) and noise (σ) of channel 13

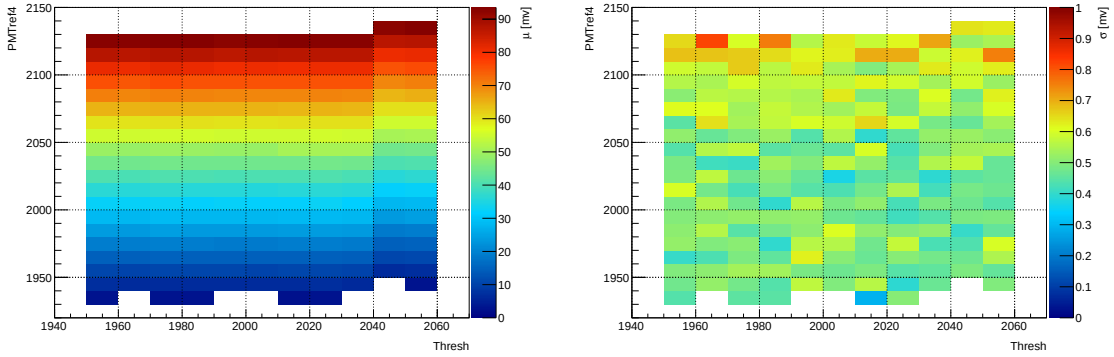

Figure 42: Mean (μ) and noise (σ) of channel 14

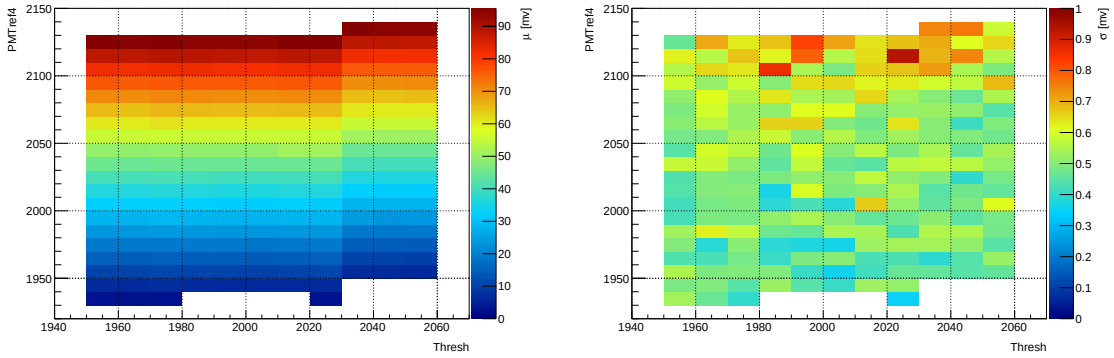

Figure 43: Mean (μ) and noise (σ) of channel 15

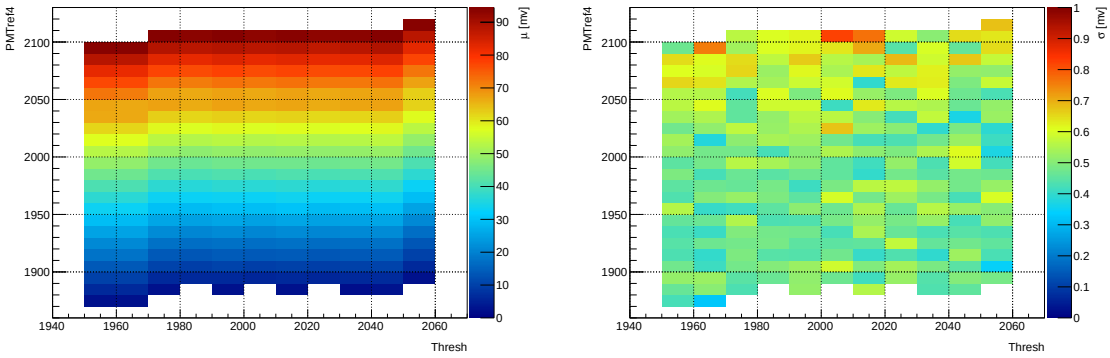

Figure 44: Mean (μ) and noise (σ) of channel 16

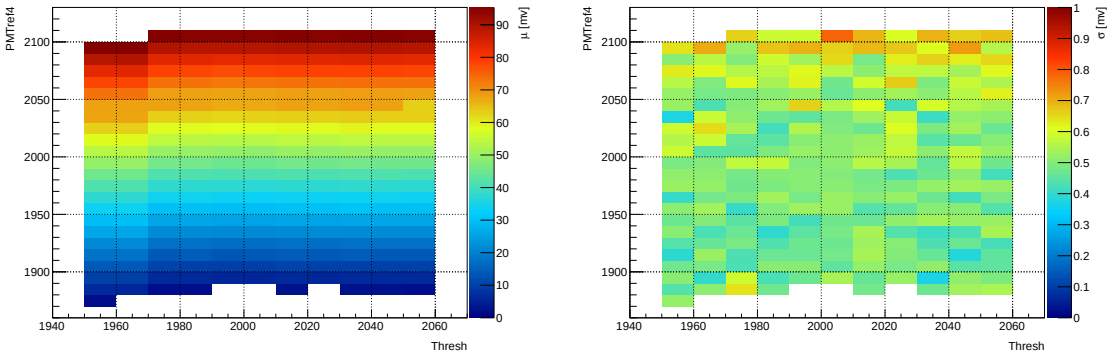

Figure 45: Mean (μ) and noise (σ) of channel 17

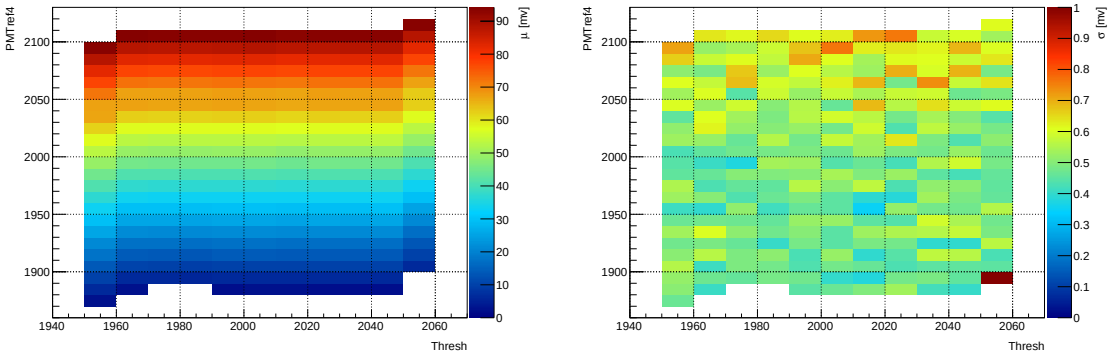

Figure 46: Mean (μ) and noise (σ) of channel 18

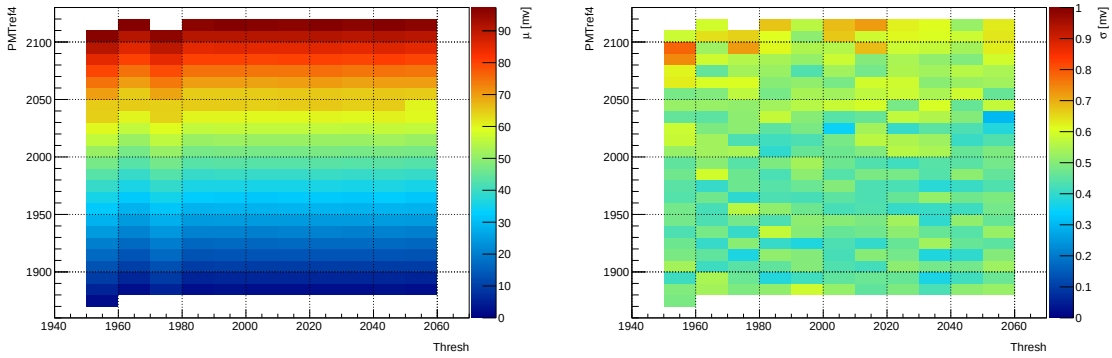

Figure 47: Mean (μ) and noise (σ) of channel 19

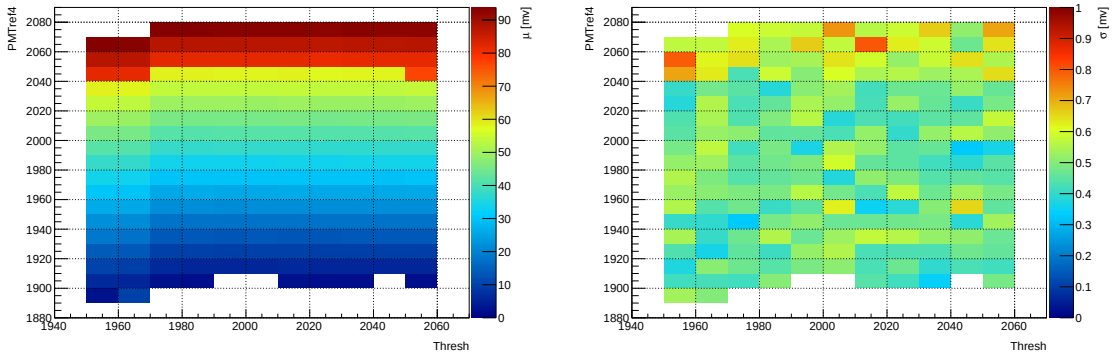

Figure 48: Mean (μ) and noise (σ) of channel 20

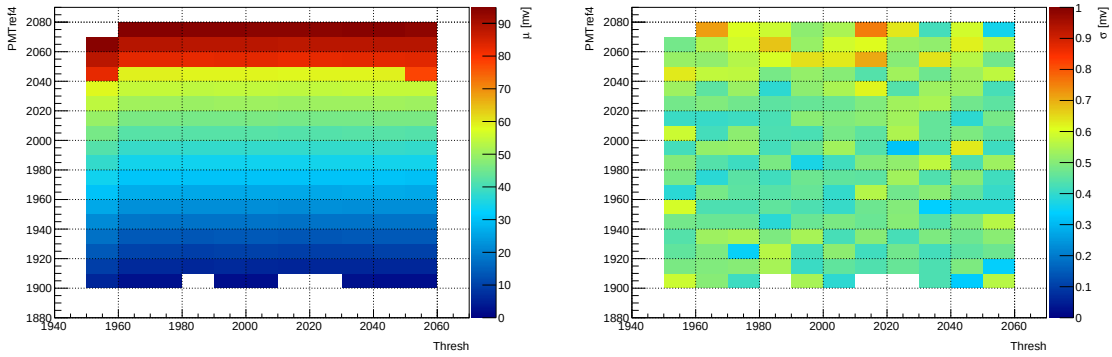

Figure 49: Mean (μ) and noise (σ) of channel 21

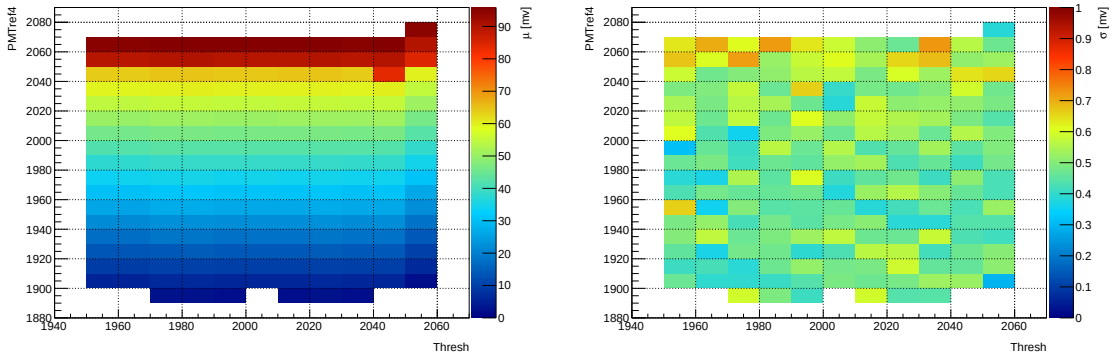

Figure 50: Mean (μ) and noise (σ) of channel 22

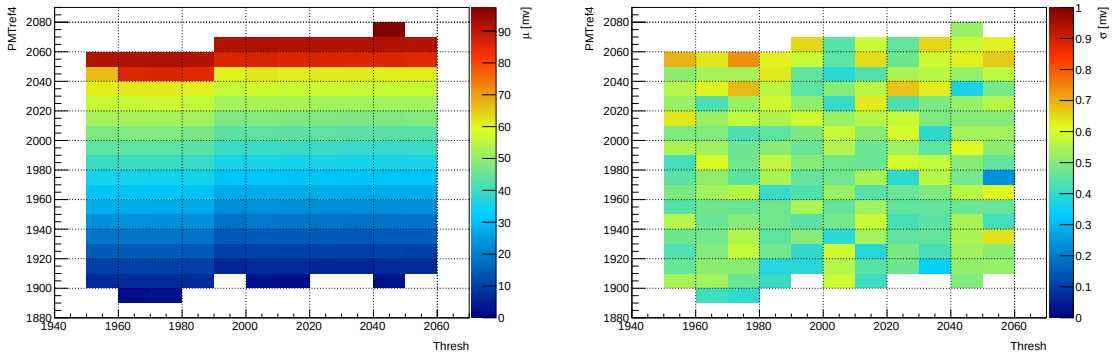

Figure 51: Mean (μ) and noise (σ) of channel 23

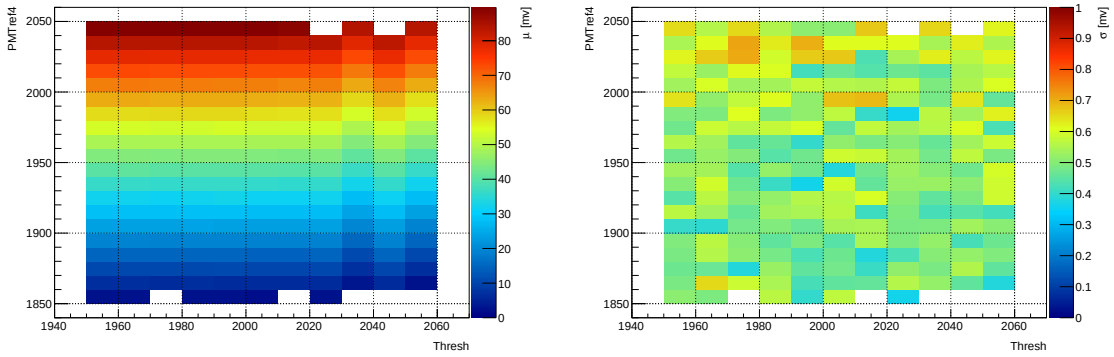

Figure 52: Mean (μ) and noise (σ) of channel 24

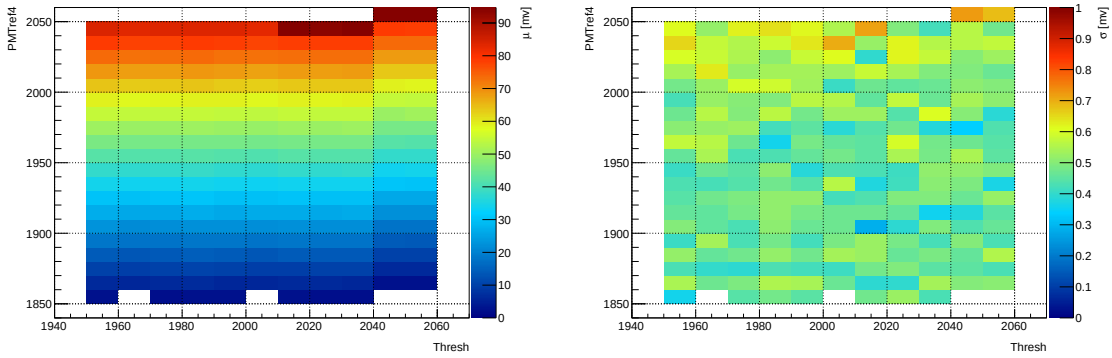

Figure 53: Mean (μ) and noise (σ) of channel 25

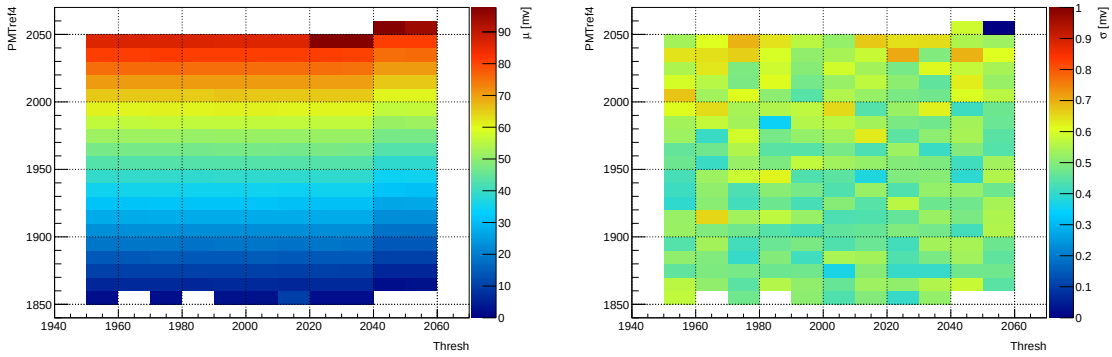

Figure 54: Mean (μ) and noise (σ) of channel 26

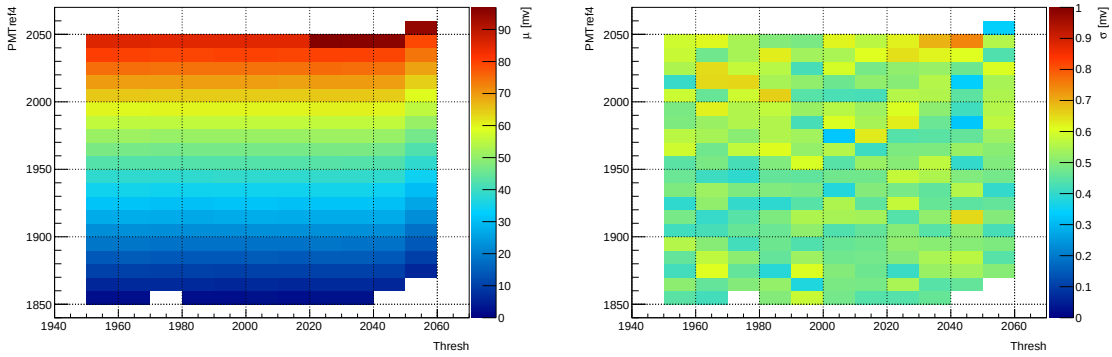

Figure 55: Mean (μ) and noise (σ) of channel 27

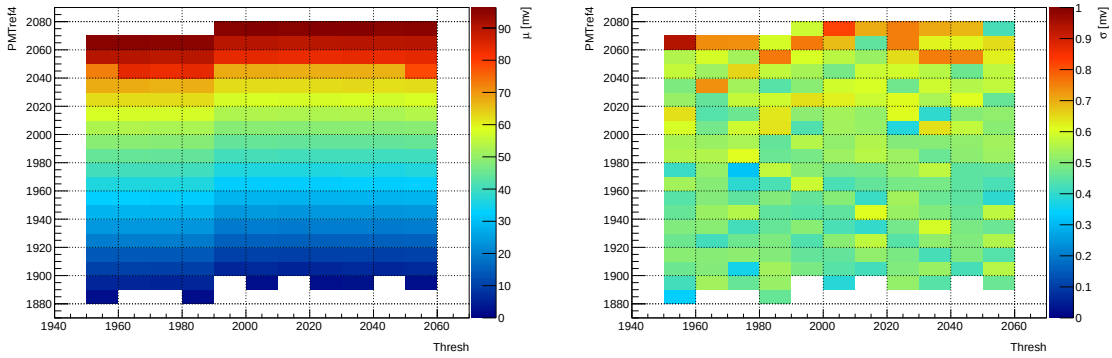

Figure 56: Mean (μ) and noise (σ) of channel 29

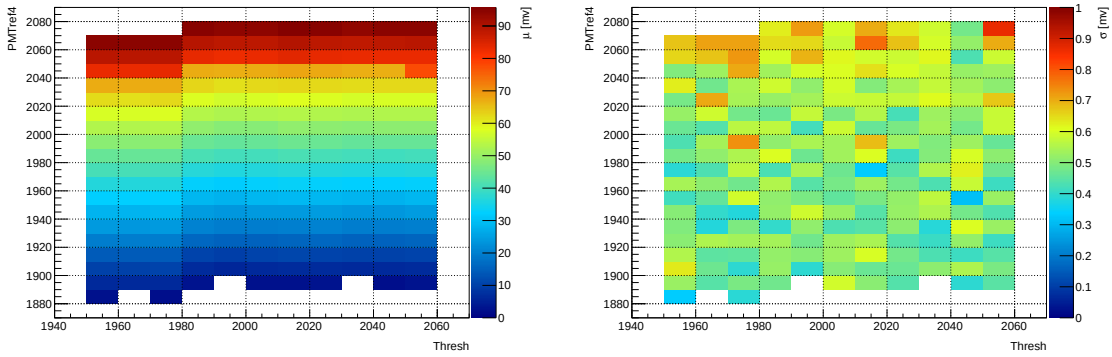

Figure 57: Mean (μ) and noise (σ) of channel 30

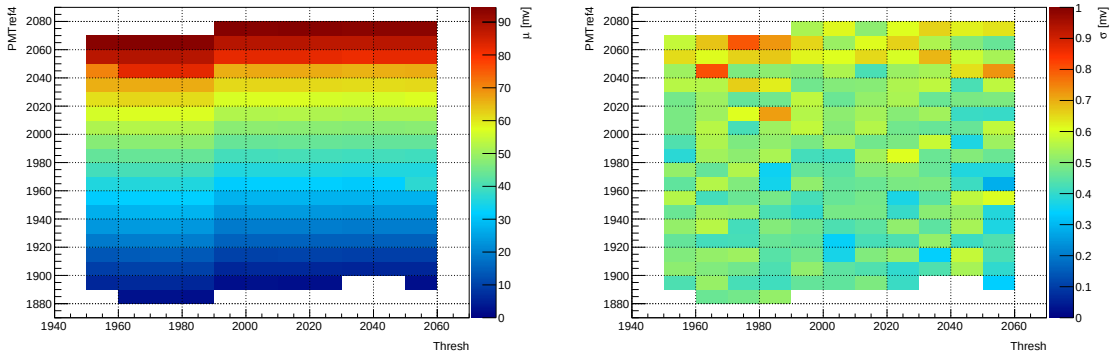

Figure 58: Mean (μ) and noise (σ) of channel 31

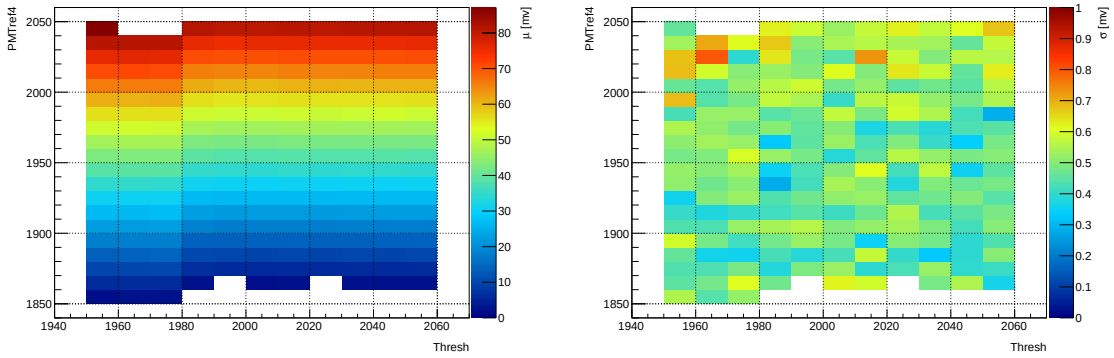

Figure 59: Mean (μ) and noise (σ) of channel 32

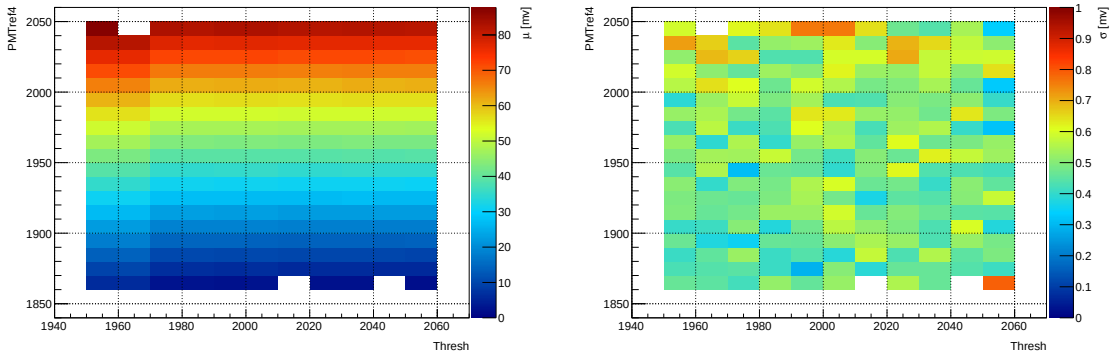

Figure 60: Mean (μ) and noise (σ) of channel 33

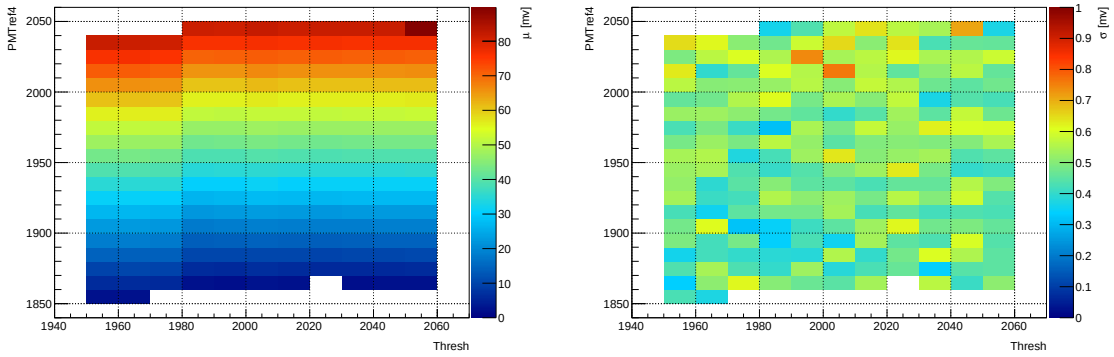

Figure 61: Mean (μ) and noise (σ) of channel 34

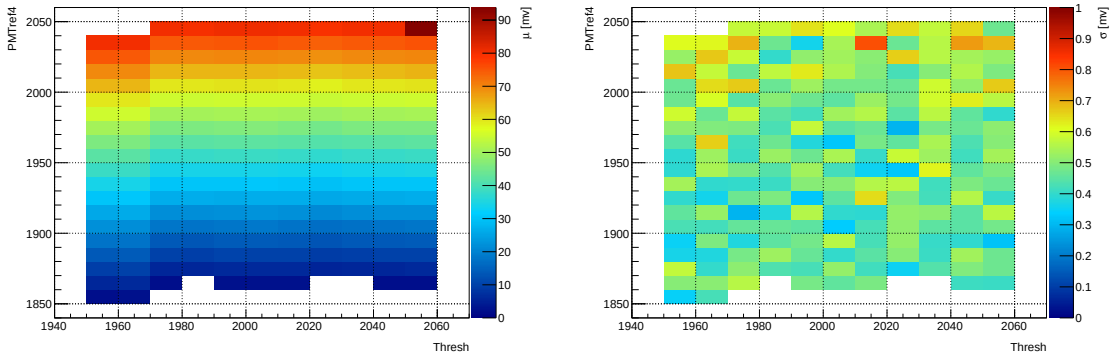

Figure 62: Mean (μ) and noise (σ) of channel 35

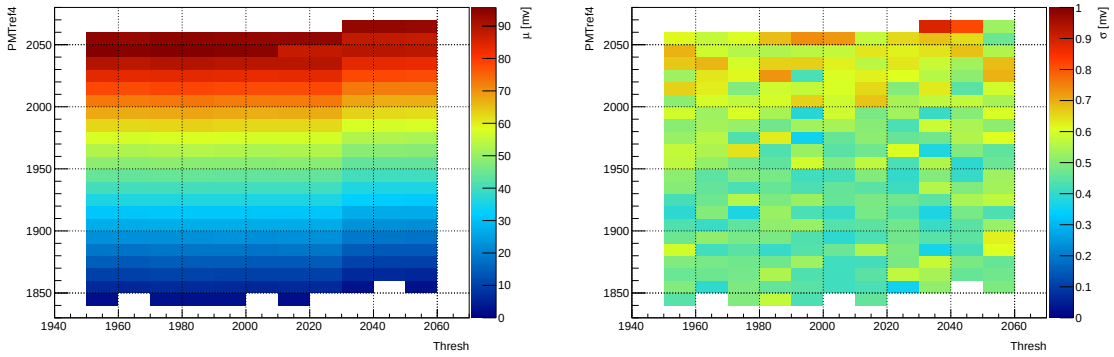

Figure 63: Mean (μ) and noise (σ) of channel 36

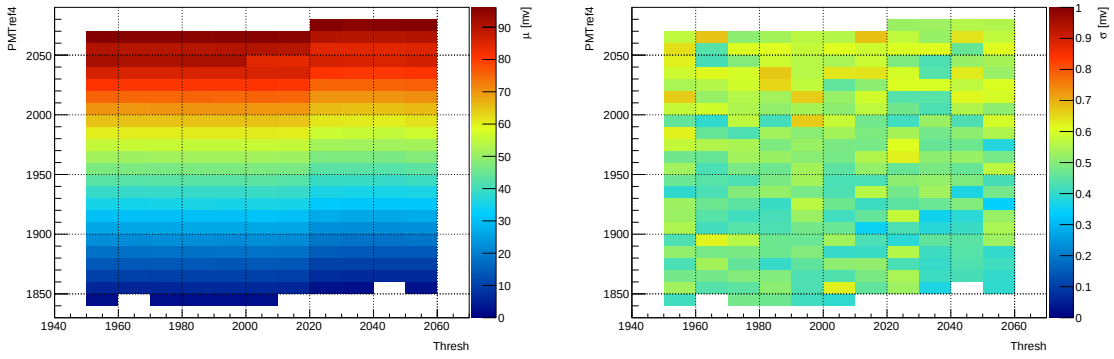

Figure 64: Mean (μ) and noise (σ) of channel 37

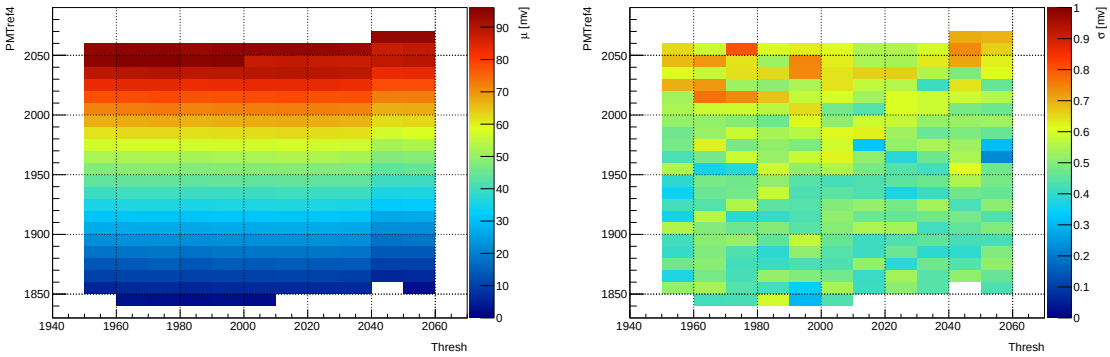

Figure 65: Mean (μ) and noise (σ) of channel 38

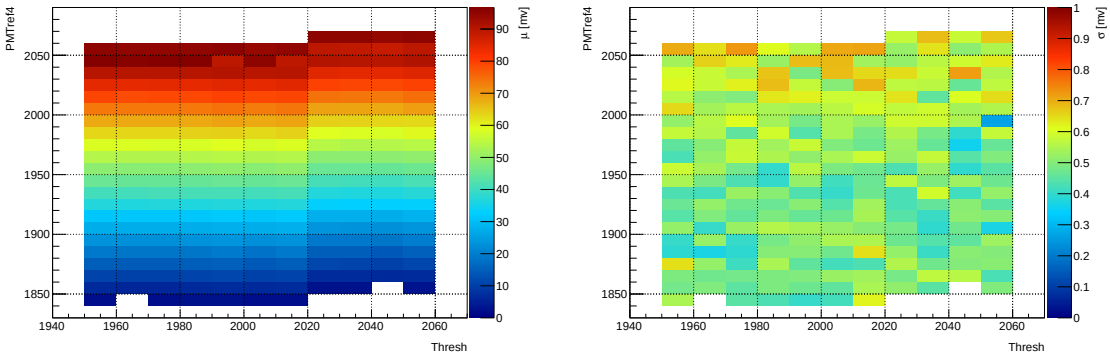

Figure 66: Mean (μ) and noise (σ) of channel 39

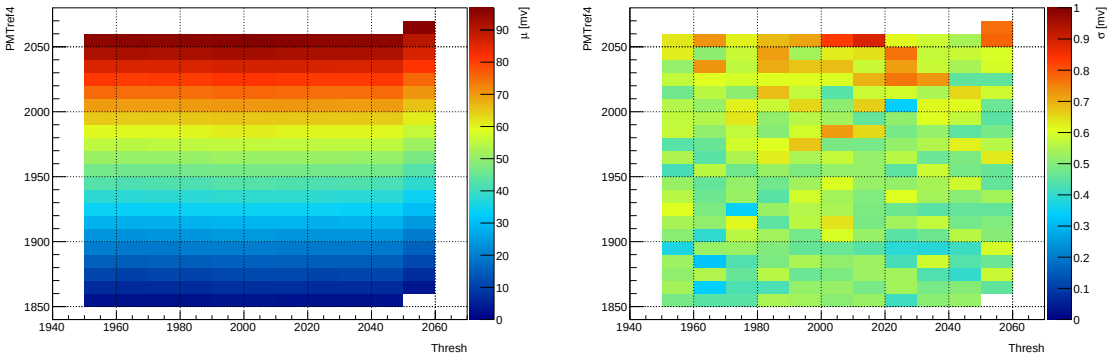

Figure 67: Mean (μ) and noise (σ) of channel 40

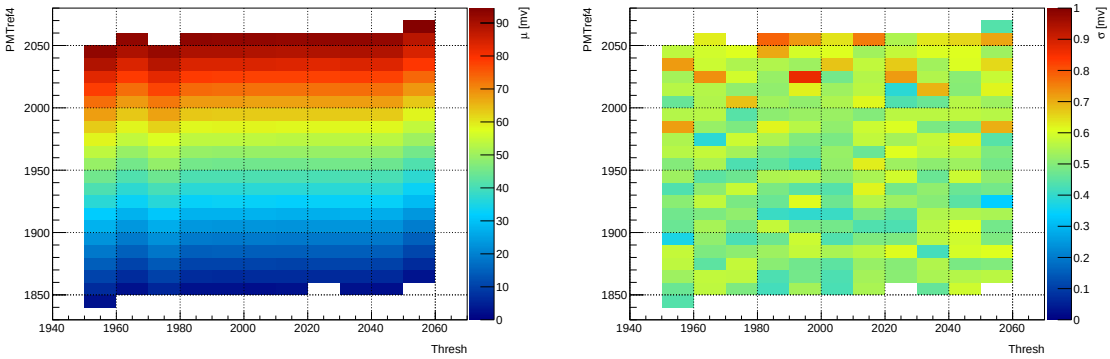

Figure 68: Mean (μ) and noise (σ) of channel 41

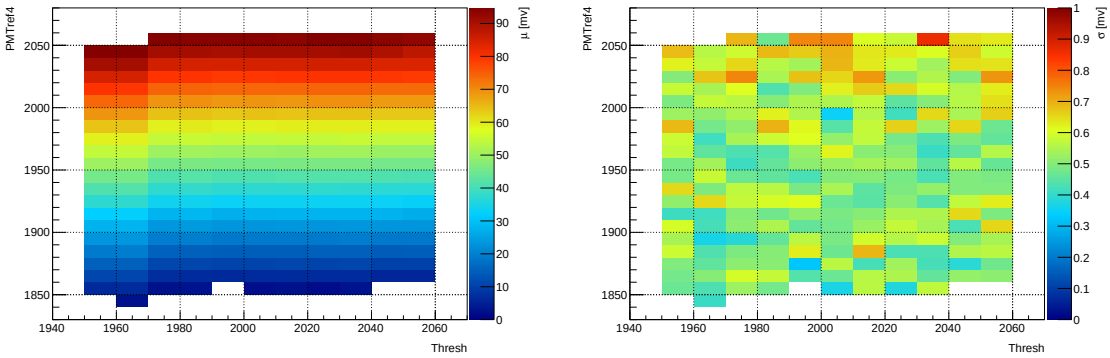

Figure 69: Mean (μ) and noise (σ) of channel 42

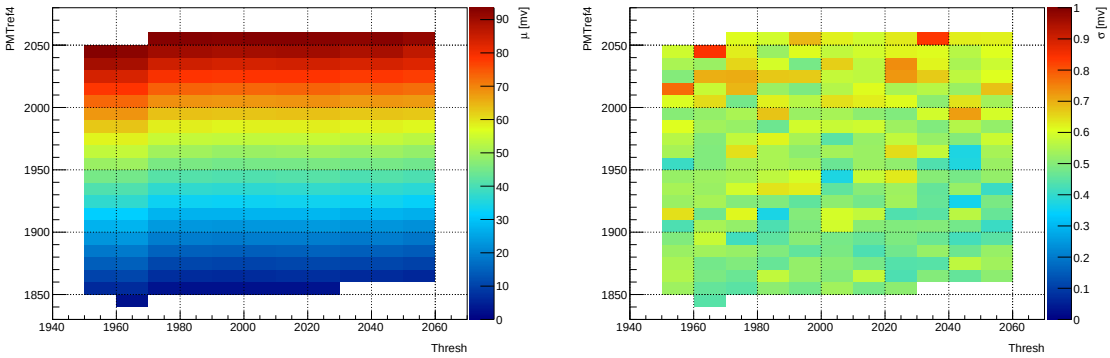

Figure 70: Mean (μ) and noise (σ) of channel 43

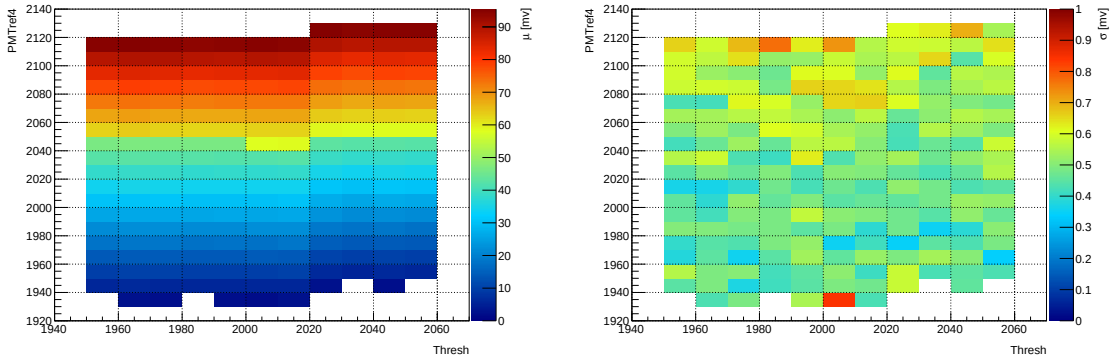

Figure 71: Mean (μ) and noise (σ) of channel 44

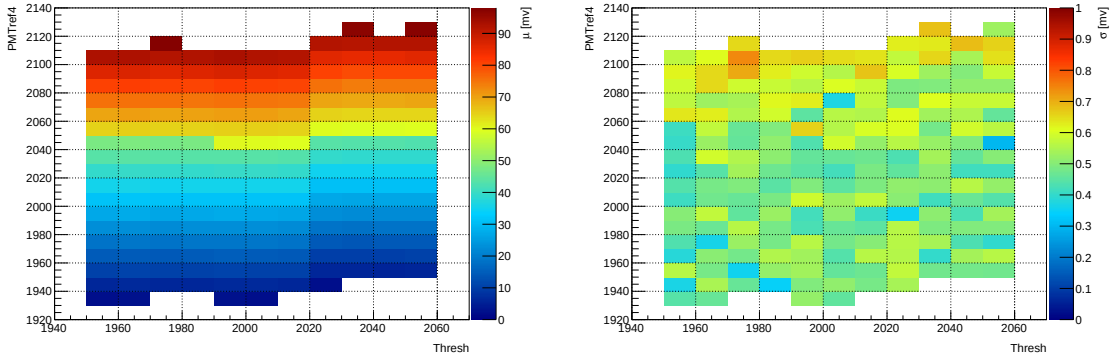

Figure 72: Mean (μ) and noise (σ) of channel 45

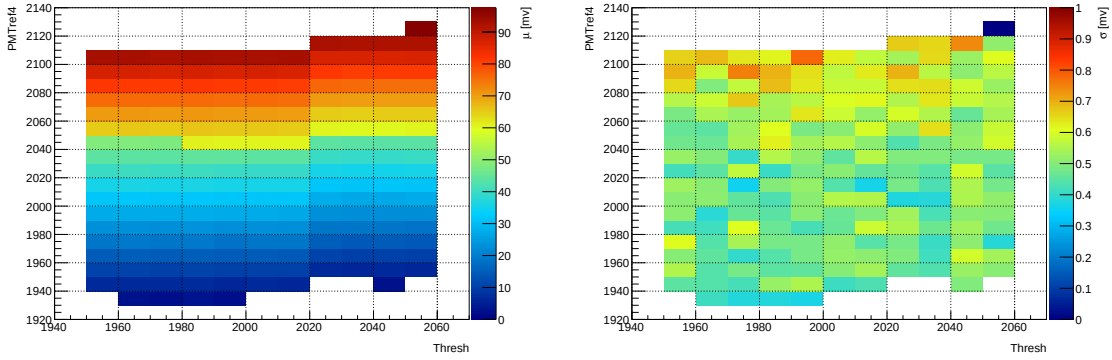

Figure 73: Mean (μ) and noise (σ) of channel 46

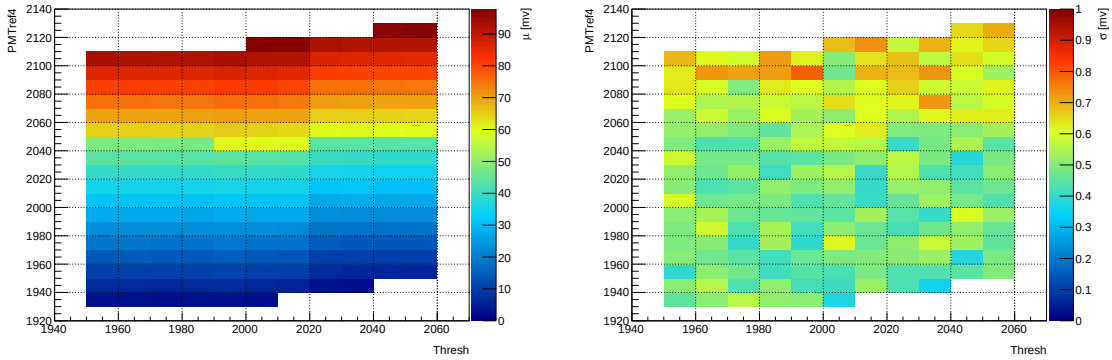

Figure 74: Mean (μ) and noise (σ) of channel 47

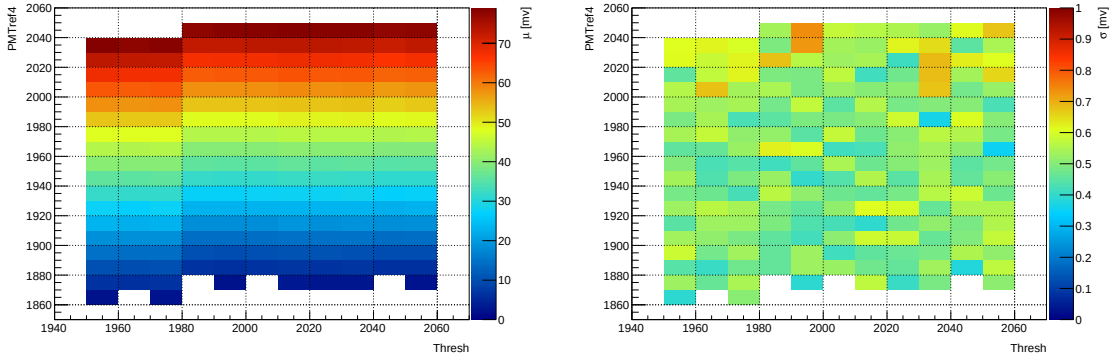

Figure 75: Mean (μ) and noise (σ) of channel 48

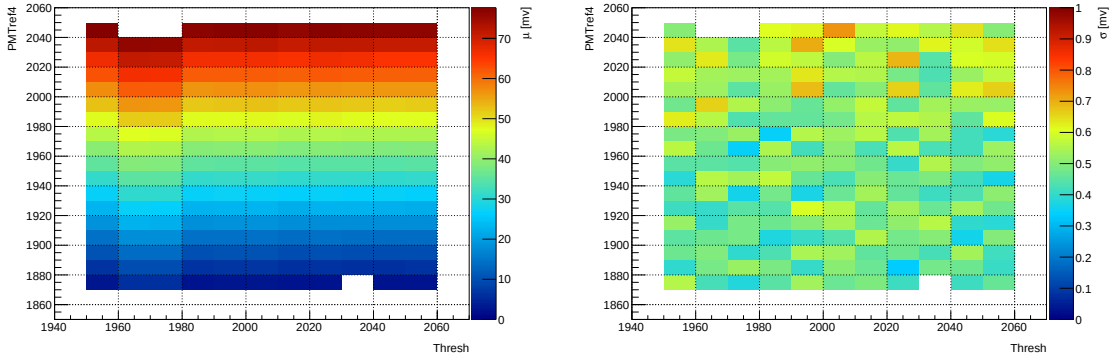

Figure 76: Mean (μ) and noise (σ) of channel 49

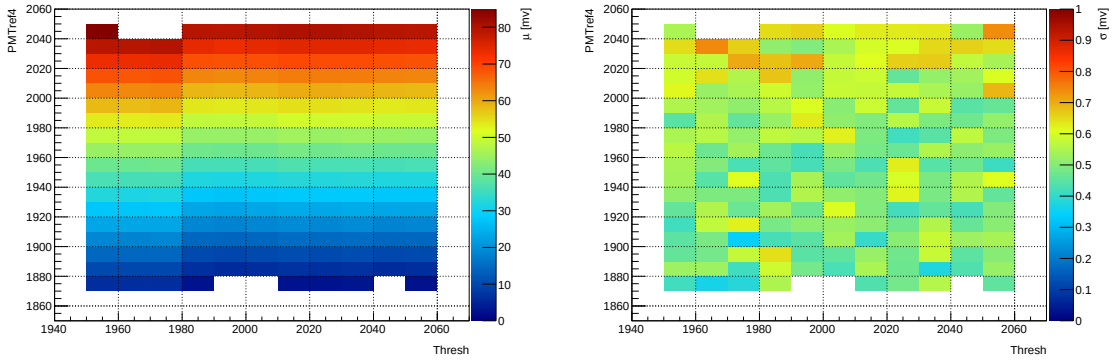

Figure 77: Mean (μ) and noise (σ) of channel 50

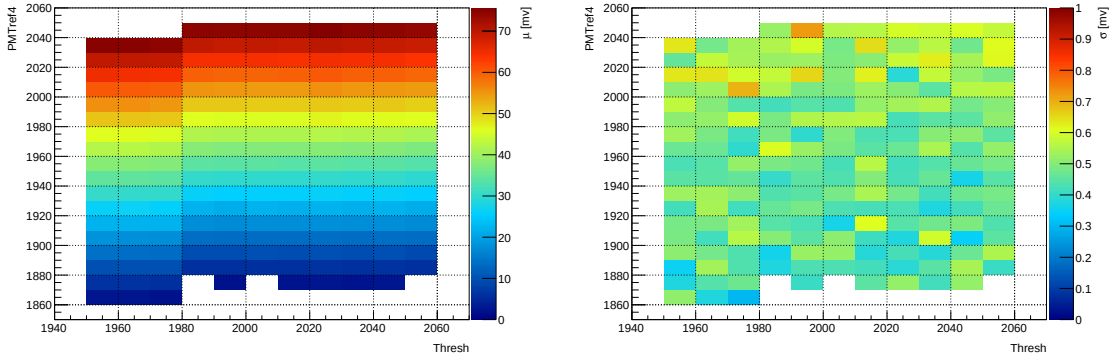

Figure 78: Mean (μ) and noise (σ) of channel 51

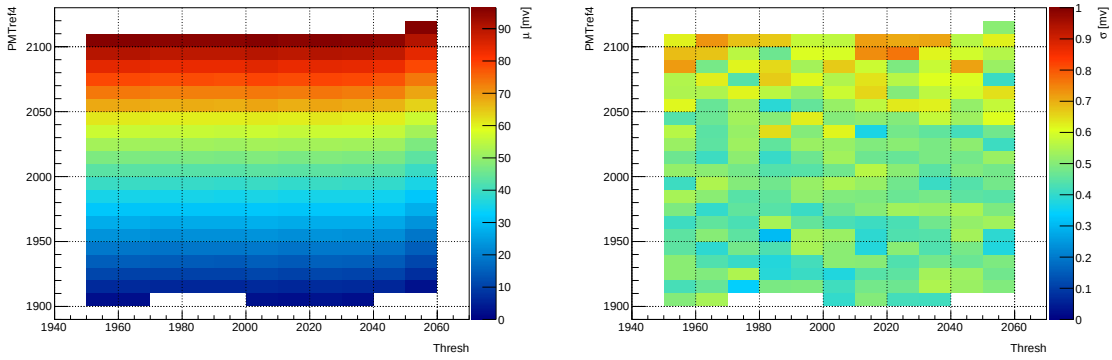

Figure 79: Mean (μ) and noise (σ) of channel 52

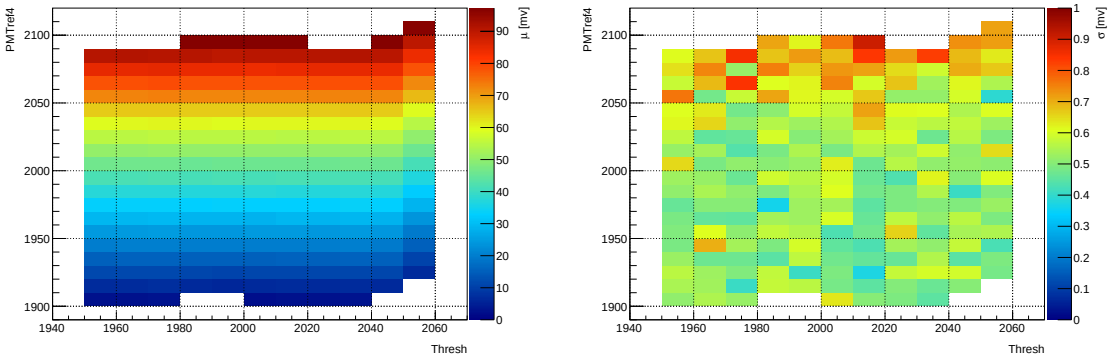

Figure 80: Mean (μ) and noise (σ) of channel 53

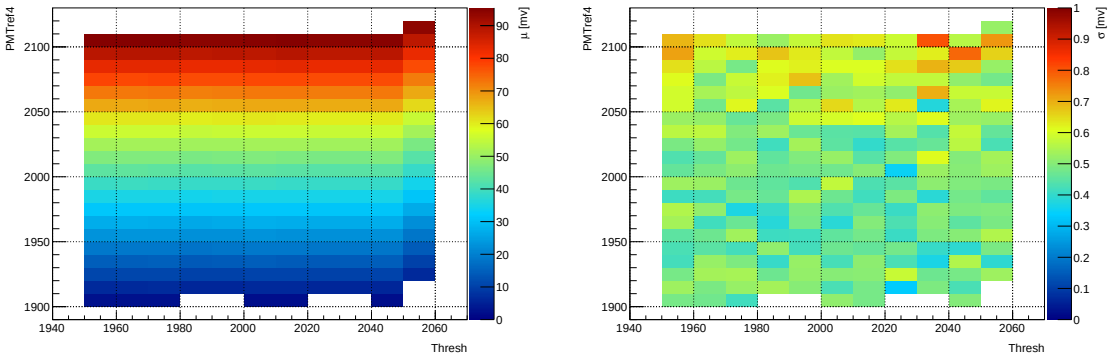

Figure 81: Mean (μ) and noise (σ) of channel 55

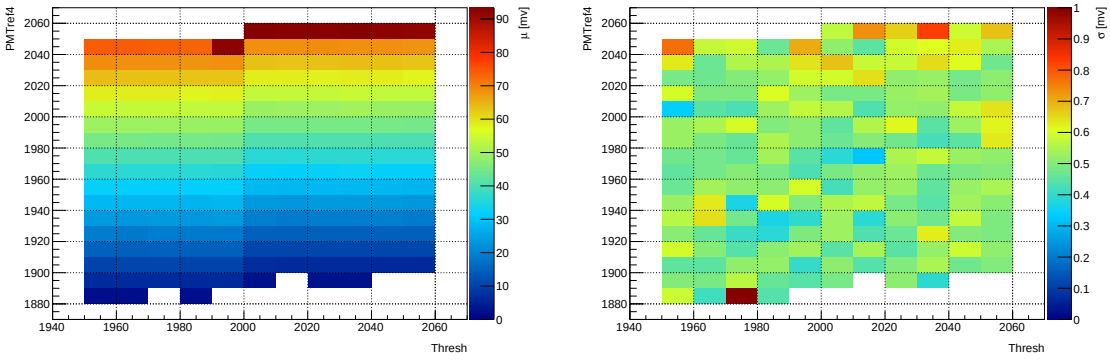

Figure 82: Mean (μ) and noise (σ) of channel 56

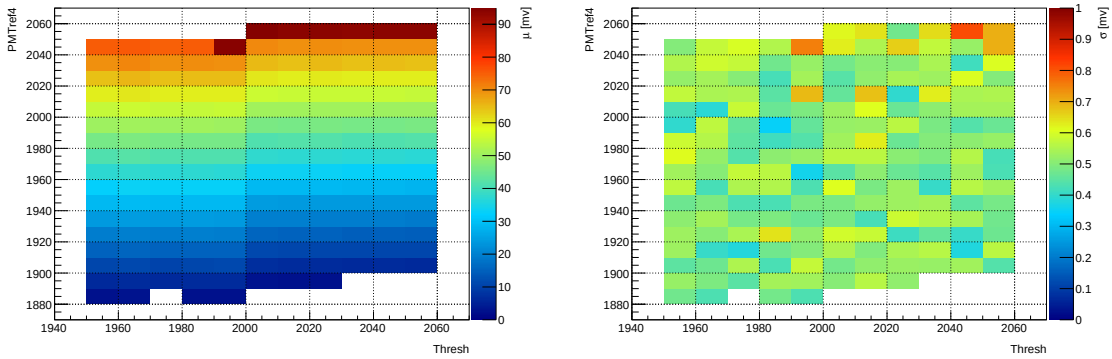

Figure 83: Mean (μ) and noise (σ) of channel 57

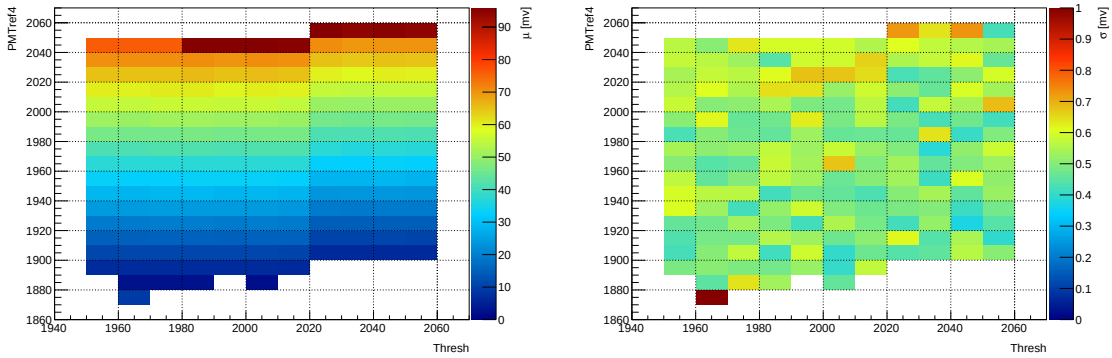

Figure 84: Mean (μ) and noise (σ) of channel 58

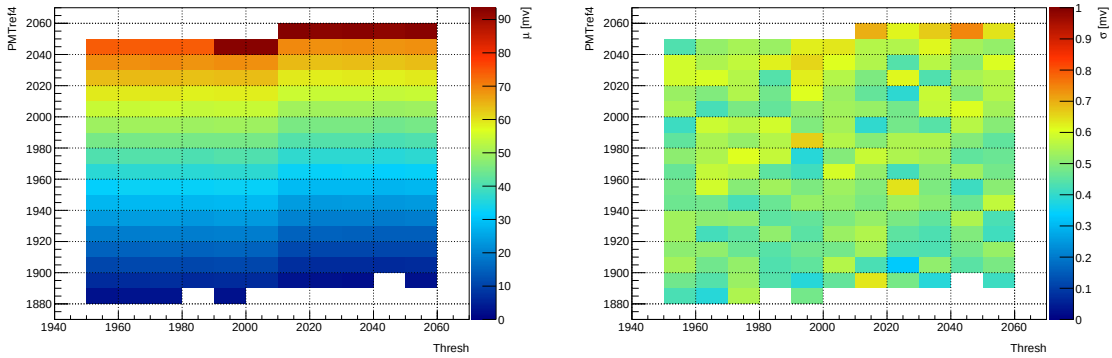

Figure 85: Mean (μ) and noise (σ) of channel 59

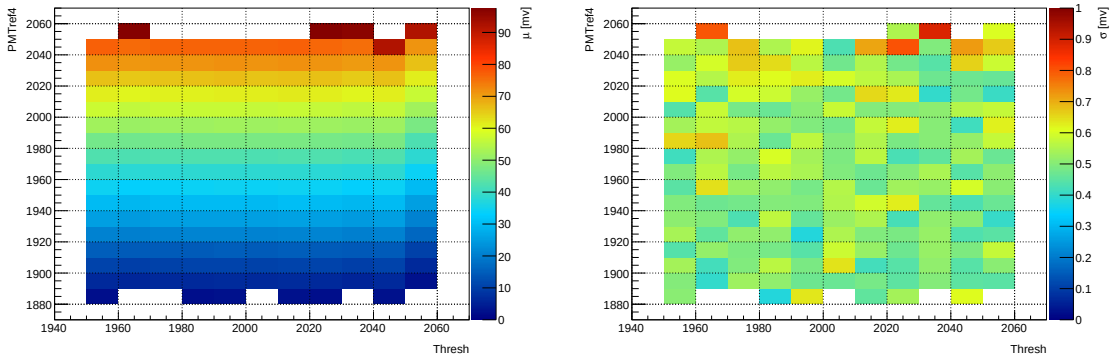

Figure 86: Mean (μ) and noise (σ) of channel 60

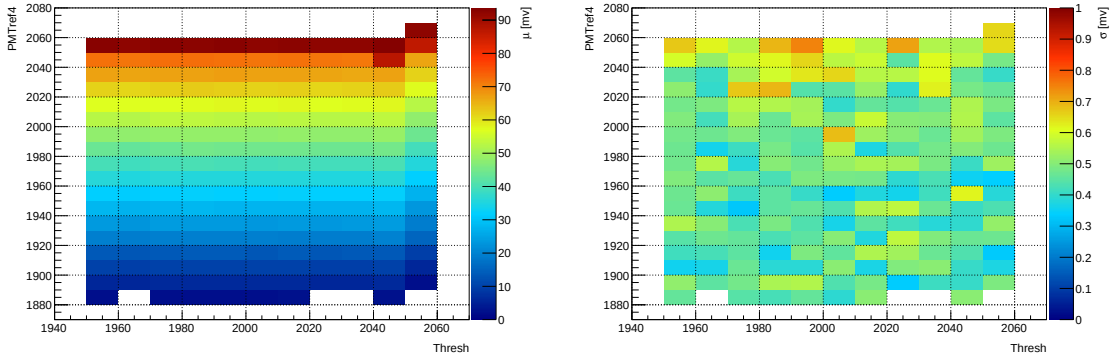

Figure 87: Mean (μ) and noise (σ) of channel 61

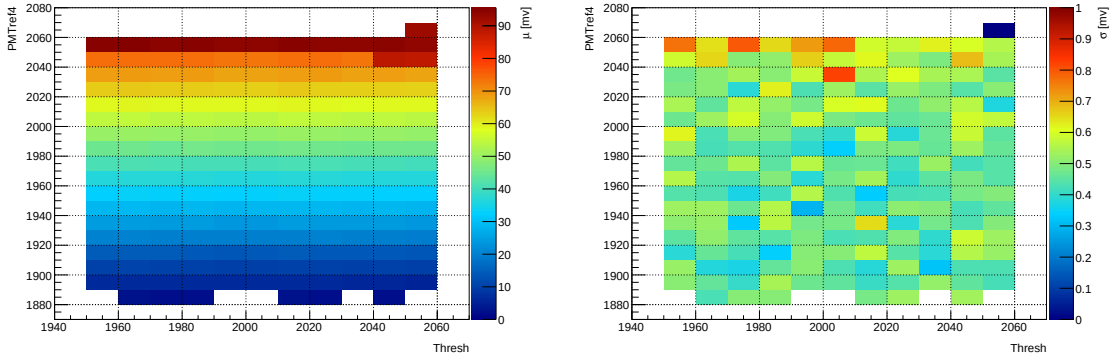

Figure 88: Mean (μ) and noise (σ) of channel 62

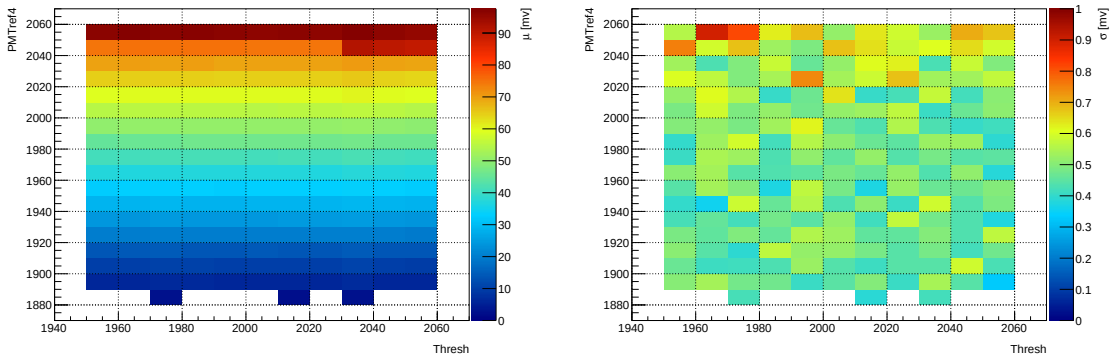

Figure 89: Mean (μ) and noise (σ) of channel 63

References

[1] NASA, The Electromagnetic Spectrum, March 2013, https://imagine.gsfc.nasa.gov/science/toolbox/emspectrum1.html

[2] NASA, Gamma-ray Astronomy, September 2013, https://imagine.gsfc.nasa.gov/science/toolbox/gamma_ray_astronomy1.html

[3] NASA, GLAST SCIENCE WRITER'S GUIDE - "Exploring the Extreme Universe", February 2008, https://www.nasa.gov/pdf/221503main_GLAST-041508.pdf

[4] NASA, Fermi, August 2008, https://www.nasa.gov/mission_pages/GLAST/multimedia/glast_rendering.html

[5] Manuel Gnida, Fermi satellite observes billionth gamma-ray with LAT instrument, May 2017, https://phys.org/news/2017-05-fermi-satellite-billionth-gamma-ray.html

[6] Wei Cui, TeV gamma-ray astronomy, *Research in Astronomy and Astrophysics*, July 2009, http://stacks.iop.org/1674-4527/9/i=8/a=001

[7] Stefan Funk, Gamma-Ray Telescope in the Classroom - Instruction manual, April 2017

[8] Max Planck Institute for Nuclear Physics, H.E.S.S., High Energy Stereoscopic System, (accessed on the 30^{th} of June, 2017) https://www.mpi-hd.mpg.de/hfm/HESS/pages/about/

[9] Max Planck Institute for Nuclear Physics, H.E.S.S., Largest ever Cherenkov telescope sees first light, (accessed on the 30^{th} of June, 2017) https://www.mpi-hd.mpg.de/hfm/HESS/pages/press/2012/HESS_II_first_light/

[10] Humboldt-Universität zu Berlin, H.E.S.S. High Energy Stereoscopic System, January 2015 https://www.physik.hu-berlin.de/de/eephys/HESS

[11] CTA Observatory, (accessed on the 9^{th} of July, 2017) https://www.cta-observatory.org

[12] M. K. Daniel, R. J. White et al., A Compact High Energy Camera for the Cherenkov Telescope Array, *33rd International Cosmic Ray Conference - ICRC 2013*, 10 July 2013, arXiv:1307.2807, https://arxiv.org/abs/1307.2807

[13] A. De Franco, R. White et al., The first GCT camera for the Cherenkov Telescope Array, *34th International Cosmic Ray Conference - ICRC 2015*, 4 September 2015, arXiv:1509.01480, https://arxiv.org/abs/1509.01480

[14] J.J. Watson, A. De Franco et al., Inauguration and First Light of the GCT-M Prototype for the Cherenkov Telescope Array, *AIP Conference Proceedings*, 5 October 2016, arXiv:1610.01452, https://arxiv.org/abs/1610.01452

[15] R. White, H. Schoorlemmer, A Compact High Energy Camera (CHEC) for the Gamma-ray Cherenkov Telescope of the Cherenkov Telescope Array, *35th International Cosmic Ray Conference - ICRC 2017*, July 2017

[16] Adrian Zink, GCT Camera CHEC-S TC Module Test Plan, 21 June 2017

[17] S. Funk, D. Jankowsky et al., TARGET: A Digitizing And Trigger ASIC For The Cherenkov Telescope Array, *AIP Conference Proceedings*, 5 October 2016, arXiv:1610.01536, `https://arxiv.org/abs/1610.01536`

[18] Johannes Schäfer, Parameter optimization of the T5TEA–ASIC for the Cherenkov Telescope Array, December 2016

[19] Jacqueline Catalano, Characterization of a custom designed trigger ASIC (T5TEA) for the Cherenkov Telescope Array, 10 August 2016

[20] David Jankowsky, Personal information

[21] Adrian Zink, Personal information

Danksagung

Zum Schluss möchte ich mich noch bei all denjenigen bedanken, die zum Gelingen dieser Arbeit beigetragen haben:

- **Prof. Dr. Stefan Funk** für die Aufnahme in die Arbeitsgruppe und die Vergabe des Themas für diese Arbeit.
- **Adrian Zink** für die Beutreuung und Hilfe bei Problemen.
- **David Jankowsky** für die Hilfe bei Problemen und das Korrekturlesen.
- **Jacqueline Catalano** für die Unterstützung beim Einarbeiten und die super Zusammenarbeit.
- **Manuel Loos** für die Hilfe beim Auf- und Umbau des Versuchs und sonstigen Problemen.
- **Johannes Schäfer** für die Hilfe beim Einarbeiten und bei Softwareproblemen.
- **Meiner Familie** für die Unterstützung bei bei meinem bisherigen Studium und meinem gesamten Lebensweg. Außerdem für die vielen Ratschläge und das wieder Aufbauen in schwierigen Phasen.

Erklärung

Hiermit bestätige ich, dass ich diese Arbeit selbstständig und nur unter Verwendung der angegebenen Hilfsmittel angefertigt habe.

Erlangen, den 14. 08. 2017